A THESIS SUBMITTED TO
THE GRADUATE SCHOOL OF NATURAL AND APPLIED SCIENCES
OF ÇANKIRI KARATEKIN UNIVERSITY

OPTIMIZATION OF BORIC ACID REMOVAL WITH GRAPHENE OXIDE SAMPLES

IN PARTIAL FULFILLMENT OF THE REQUIREMENTS
FOR
THE DEGREE OF MASTER OF SCIENCE
IN
CHEMICAL ENGINEERING

BY

TABAREK SALAM MAJEED MAJEED

ÇANKIRI

2024

OPTIMIZATION OF BORIC ACID REMOVAL WITH GRAPHENE OXIDE SAMPLES

By Tabarek Salam Majeed MAJEED

January 2024

We certify that we have read this thesis and that in our opinion it is fully adequate, in scope and in quality, as a thesis for the degree of Master of Science

Advisor **:** Asst. Prof. Dr. Haluk KORUCU
Co-Advisor **:** Res. Asst. Dr. Esra YILMAZ MERTSOY

Examining Committee Members:

Chairman **:** Prof. Dr. Ahmet YARTAŞI
Chemical Engineering
Çankırı Karatekin University

Member **:** Assoc. Prof. Dr. Nejdet DEĞERMENCİ
Environmental Engineering
Kastamonu University

Member **:** Asst. Prof. Dr. Haluk KORUCU
Chemical Engineering
Çankırı Karatekin University

Approved for the Graduate School of Natural and Applied Sciences

Prof. Dr. Hamit ALYAR
Director of Graduate School

I hereby declare that all information in this document has been obtained and presented in accordance with academic rules and ethical conduct. I also declare that, as required by these rules and conduct, I have fully cited and referenced all material and results that are not original to this work.

Tabarek Salam Majeed MAJEED

ABSTRACT

OPTIMIZATION OF BORIC ACID REMOVAL WITH GRAPHENE OXIDE SAMPLES

Tabarek Salam Majeed MAJEED

Master of Science in Chemical Engineering

Advisor: Asst. Prof. Dr. Haluk KORUCU

Co-Advisor: Res. Asst. Dr. Esra YILMAZ MERTSOY

January 2024

The world's greatest reserves of boron are found in Türkiye. Boron compounds, such as boric acid, borax, boroxide, are generated in Türkiye by processing boron ores. Environmental issues come from the formation of boron waste during production operations, as this waste cannot be evaluated. This work aims to characterize the optimization of adsorption of synthetically generated boric acid solutions using graphene oxide samples by the Taguchi method. The study used the L_9 (3^4) experimental design, which has 4 factors and 3 levels. The factors that were chosen were the pH of the solution, the method used to make graphene oxide, the amount of graphene oxide that was used, and the concentration of boric acid. The Staudenmaier, Staudenmaier-Hummers, and Hummers techniques were chosen for the production of graphene oxide at pH levels of 3.5, 7, and 10. The amounts of graphene oxide used were 1g, 2g, and 3g. The experiments were conducted using the L_9 (3^4) experimental design, model. Raman spectroscopy was used to determine the D/G peak ratio in graphene oxide samples. SEM+EDS analysis was conducted to measure the C/O ratio. BET analysis was employed to measure the surface area. The zeta sizer was used to analyze the zeta potential and particle size distribution. Finally, FTIR was used for structural characterization. It was measured to see how much boric acid was left in the fluid and how much boric acid was kept per gram of graphene oxide. The Taguchi method was used to assess the adsorption of boric acid on graphene oxide samples of the criterions numerical results. Optimum points were obtained for each criterion. Due to variations in the characteristics of graphene oxide, distinct patterns have been discovered at the places that yield the best results for each criterion. When evaluating the adsorbed boric

acid per gram graphene oxide, it was noted that the retention of boric acid per gram of graphene oxide increased with higher pH levels and greater boron concentration in the solution. Additionally, the quantity of graphene oxide utilized dropped as the amount increased. The Staudenmeair method has demonstrated greater efficacy in adsorbing boric acid than the Hummers method. It's possible that graphene oxide can be used on its own for boric acid binding once the Taguchi optimization results of the $L_9(3^4)$ experimental design are looked at. Furthermore, boric acid adsorption has been shown to improve the criteria properties of graphene oxide, according to the optimization results. These findings indicate that graphene oxide is a useful material for eliminating boron industrial process waste.

2024, 70 pages

Keywords: Hummers method, Staudenmaier method, Taguchi method, Boric acid, Adsorption

ÖZET

GRAFEN OKSİT ÖRNEKLERİYLE BORİK ASİT GİDERİMİNİN OPTİMİZASYONU

Tabarek Salam Majeed MAJEED
Kimya Mühendisliği, Yüksek Lisans
Tez Danışmanı: Dr. Öğr. Üyesi. Haluk KORUCU
Eş Danışman: Arş. Gör. Dr. Esra YILMAZ MERTSOY
Ocak 2024

Türkiye dünyanın en büyük bor rezervlerine sahip ülkesidir.Türkiye de bor cevherlerini işlenerek borik asit, boraks, boroksit gibi bor bileşikleri üretilmektedir. Üretim süreçlerinde prosesler içinde bor atığı oluşmakta, bu atığın değerlendirilmesi mümkün olmadığı için çevresel sorunlar ortaya çıkmaktadır. Bu çalışmada sentetik olarak hazırlanan borik asit çözeltilerinin, grafen oksit örnekleri ile adsorbsiyonun Taguchi yöntemi ile optimizasyonun karakterize edilmesi hedeflenmiştir. Çalışmamızda 4 parametre ve 3 seviyeden oluşan L_9 (3^4) deney tasarımı kullanılmıştır. Seçilen parametreler çözelti pH, grafen oksit sentez yöntemi, grafen oksit miktarı ve borik asit konsanstrasyonu olarak belirlenmiştir. pH olarak 3,5-7-10, grafen oksit sentez yöntemi olarak Staudenmaier, Staudenmaier-Hummers, Hummers yöntemleri, grafen oksit miktarı olarak 1g, 2g, 3g olarak seçilmiştir. L_9 (3^4) deney tasarımı modeline gore deneyler gerçekleştirilmiştir. Her deney sonunda grafen oksit örnekler ve çözeltisi birbirinden ayrılarak analiz edilmiştir. Grafen oksit örneklerinde Raman ile D/G pik oranı ,SEM +EDS ile C/O oranı, BET ile yüzey alanı ölçümü, ZETA SİZER ile Zeta potansiyeli ve parçacık boyut dağılım analizi ve FTIR ile yapı karakterizasyonu gerçekleştirilmiştir. Çözeltide ise kalan borik asit analiz edilerek gram grafen oksit başına tutulan, borik asit hesap edilmiştir. Grafen oksit örneklerine ait ve borik asit adsorplanmasına yönelik sayısal sonuçlar, Taguchi yöntemi ile analiz edilerek her bir kriter için optimum noktalar belirlenmiştir. Grafen oksit özelliklerini ilgilendiren kritler birbirlerinden farklı davranış gösterdiği için, kriterlere gore optimum noktlarda farklılıklar gözlenmiştir. Gram grafen oksit başına adsorblanan borik asit değerlendirildiğinde, pH artıkça ve çözeltideki bor miktarı artıkça gram grafen oksit

başına tutulan borik asit miktarının artığı ve kullanılan grafen oksit miktarı artıkçada azaldığı gözlenmiştir. Staudenmeair yönteminın, Hummers yöntemine gore borik asit adsorbsiyonu üzerinde daha başarılı olduğu gözlenmiştir. $L_9(3^4)$ Deney tasarımına ait Taguchi optimzasyon sonuçları değerlendirildiğinde, grafen oksitin borik asit adsorbsiyonunda tek başına kullanılabilmesi mümkündür. Ayrıca borik asit adsorbsiyonun grafen oksitin kriter özelliklerinde iyileştirici etkilerde bulunduğu optimizasyon sonuçlarındanda görülmüştür. Bu sonuçlar grafen oksitin bor tesisleri proses atıklarının gideriminde de kullanılabilirliğini gösteren nitelikte bir çalışma olmuştur.

2024, 70 sayfa

Anahtar Kelimeler: Hummers yöntemi, Staudenmaier yöntemi, Taguchi yöntemi, Borik asit, Adsorpsiyon

PREFACE AND ACKNOWLEDGEMENTS

I humbly dedicate this thesis to the members of my thesis committee for their insightful guidance and direction.

First and foremost, I dedicate this work to my adviser Asst. Prof. Dr. Haluk KORUCU, who chaired my thesis committee. His leadership and supervision throughout this project was invaluable. I also dedicate this thesis to my Co-Advisor : Res. Assist. Dr. Esra YILMAZ MERTSOY, committee member, for his dedication in consistently monitoring my progress and providing constructive feedback. This work would not have been possible without their mentorship, guidance and for graciously providing their precious time to ensure the completion of this thesis.

I also dedicate this to my loving family, my precious mother Ilham Neamah, my father Salam Majeed, my sister Sara Salam, and my brother Ali Salam, for their continual support throughout my years of study, and who are always a source of strength and love for me.

And I express my deepest gratitude to Çankırı Karatekin University for providing all means of support and facilities.

It is my hope that this thesis contributes, in some way, to advancing research in this field.

Tabarek Salam Majeed MAJEED

Çankırı-2024

CONTENTS

LIST OF SYMBOLS

cm	Centimeter
ºC	Degree celsius
g	Gram
g/mL	Gram per milliliter
h	Hour
mg/L	Milligrams per liter
min	Minute
mg/g	Milligrams per gram
mL	Milliliter
mV	Millivolt
µm	Micrometer
Nm	Nanometer
ppm	Parts per million
pp	Parts per billion
m^2/g	Square meter per gram

LIST OF ABBREVIATIONS

ACrGO	Activated chromium-modified reduced graphene oxide
Al	Aluminum
B_2O_3	Boron oxide
H_3BO_3	Boric acid
BET	Brunauer–emmett–teller surface area
Cr	Chromium
D/G	Carbon-to-oxygen ratio
C/O	Carbon-oxygen ratio
EDX	Energy-dispersive x-ray spectroscopy
FESEM	Field-emission scanning electron microscopy
FTIR	Fourier transform infrared spectroscopy
GEO	Graphene oxide exfoliated
GO	Graphene oxide
GO-Amnt	Graphene oxide amount
H_2O_2	Hydrogen peroxide
HCl	Hydrochloric acid
ID/IG	Intensity ratio of d peak to g peak
Fe	Iron
Fe_3O_4	Iron (II,III) oxide
MB	Methylene blue
MOFs	Metal-organic frameworks.
HNO_3	Nitric acid
PS	Particle size
PSD	Particle size distribution
$KClO_3$	Potassium chlorate
$KMnO_4$	Potassium permanganate
H_3PO_4	Phosphoric acid
R	Reaction
rGO	Reduced graphene oxide
rGO-Ag	Reduced graphene oxide-silver
GO/Cu4	Reduced graphene oxide-copper
AgNPs	Silver nanoparticles
H_2SO_4	Sulfuric acid
NaOH	Sodium hydroxide
GO-SH	Synthesis of graphene oxide from graphite using the Staudenmaier-Hummers method
GO-H	Synthesis of GO (graphene oxide) from graphite using the modified Hummers method

GO-S	Synthesis of graphene oxide from graphite using the Staudenmaier method
SEM-EDS	Scanning electron microscope - energy dispersive spectroscopy
SA	Surface area
S/N	Signal to noise ratio
3D	Three-dimensional
TGA	Thermogravimetric analysis
TEM	Transmission electron microscopy
XRD	X-ray diffraction
XPS	X-ray photoelectron spectroscopy
ZP	Zeta potential

LIST OF FIGURES

LIST OF TABLES

1. INTRODUCTION

1.1 Allotropes of Carbon

Carbon is essential for life because it is found in all living organisms on Earth. It is one among the elements in Periodic Table Group IV. It has four electrons available in its outermost orbit. Covalent chemical bonds are formed by these electrons. It possesses distinctive chemical characteristics. Carbon atoms can create lengthy chains by combining with other carbon atoms. It has various allotropes such as graphite, diamond, fullerene, carbon nanotubes, and graphene (Kharisov and Kharissova 2019) as shown in Figure 1.1. Carbonaceous compounds and carbon allotropes are materials of significant scientific and technological importance. Notably, their zero-, one-, and two-dimensional species and constructs are currently being investigated as key components of advanced materials for a wide range of applications, including nano- and optoelectronics, photonics, molecular separation and storage, nano mechanics, catalysis, and energy storage (Lin *et al.* 2018).

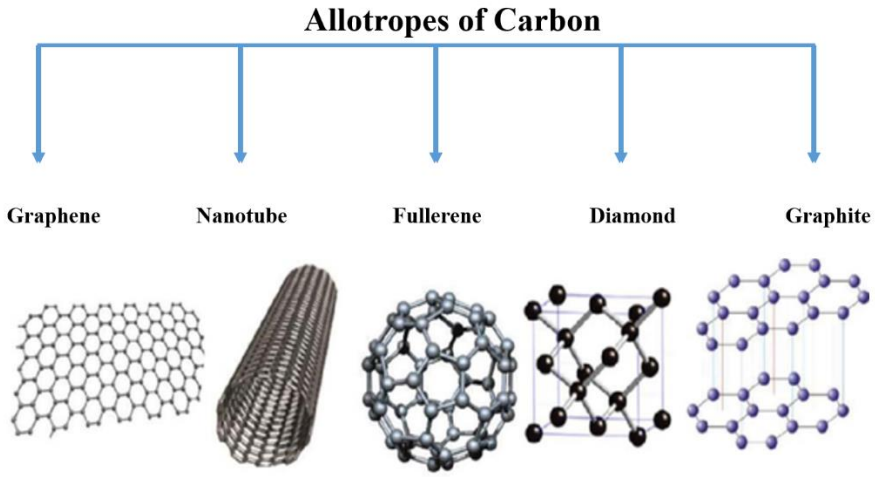

Figure 1.1 Crystal structures of different carbon allotrope (Kharisov and Kharissova 2019)

1.1.1 Graphite

In this carbon allotrope type ‘graphite’, carbon atoms arranged in regular hexagons with a 120- degree C-C-C bond angle and graphite has sp^2 hybridization. Carbon atoms form sheets of six sided rings with p-orbitals perpendicular to the ring plane. Carbon atoms share three of their four valence electrons with their three nearest neighbors. The remaining electron in the out of plane p-orbital is delocalized and this allow the weak Van der walls forces to hold the sheets together. These sheets are more susceptible to separate because of the weak forces that hold the sheets together. The distance between the layers of graphite is 0.334 nanometers. Since graphite has different properties in its direction, it is considered to be an anisotropic material. Due to covalent and metallic bonds within a carbon layer, it possesses high electrical and thermal conductivity. In contrast, the electric and thermal conductivity perpendicular to the carbon layers is poor (Kharisov and Kharissova 2019).

1.1.2 Diamond

Diamond is another carbon allotrope type (within 3-D) where carbon atoms are bonded with sp^3 hybridization in tetrahedral crystal structure. Each carbon atom attaches to four other carbon atoms and separated by a distance 0.154 nm. The angle of the bond between the C-C-C is 109.5^o. Strong covalent bonds are created among each carbon atom and the four neighbor carbon atoms. For this reason, diamond is considered to be the hardest materials and it’s tough to break carbon atoms apart and thus exhibits high resistance to compression. In addition, diamond has excellent photonic and heat conductivity but lacks to be electrically conductive. It is optically transparent with a wide range spectrum from ultraviolet to infrared light. Moreover, it is chemically stable and shows low adhesion characteristic with other solids which resulted in low friction and wear. Diamond withstands with high temperature environment up to 1000 ^OC under atmospheric pressure and 1400 ^OC under vacuum but it transforms to graphite beyond these conditions (Honda *et al.* 2021).

1.1.3 Fullerene

Fullerene, which is the first molecular carbon allotropes, is discovered in 1985 in its gas phase form. Also, fullerene synthesis discovery utilizing arc vaporization of graphite in 1990 have sparked upsurge of contemporary chemistry (Ahmad *et al.* 2020). Noble prize was awarded for 1.1.3 fullerene discovery in 1996. Fullerene's structure is like graphite, but fullerene composed of stacked graphene sheets in hexagonal or pentagonal structure. C_{60} (or buckyballs), which is the most common fullerene family members, has superior chemical and physical properties in addition to its spherical shape and unequalled in nature which resulted in its widespread use as lubricants, catalysts, superconductors, and photoconductors (Pan *et al.* 2020). Scaling-up the fullerene has faced some obstacles as it is insoluble or low soluble in most solvents and easy to aggregate which makes the case worse. This can be partially solved with the aid of fullerene's functionalization (Kunkel *et al.* 2020).

1.1.4 Carbon nanotube

Carbon nanotubes (CNTs) are 1-D nanomaterials that exist as single-walled carbon nanotubes (SWCNTs) or multi-walled carbon nanotubes (SWCNTs) structures which wrapped in a cylindrical shape. CNTs features depend on the morphology, tube geometry, nano structure, and the atomic arrangement (how the graphite sheets are rolled) (Dai, Li, and Fan 2021). CNTs has attracted much interest of researchers due to their electrical, thermal, and physical properties. For instance, CNTs are thermally stable up to 2800 ^{O}C under vacuum (its thermal conductivity 2-fold of diamond's conductivity), carrying the electrical current (1000 times higher than copper wires). High specific surface area and strong Van der Waals forces between the nanocarbon particles resulted in highly particles agglomeration. Also, CNTs is considered to be hydrophobic which hinder their dispersion in aqueous suspensions. CNTs are long and slim fullerene where the tubes wall is hexagonal carbon in graphite structure and often closed at each end. CNTs have exceptional mechanical features such as high elastic modulus and high strength (Merodio-Perea *et al.* 2022).

1.1.5 Graphene

Graphene or graphene nanoplatelets (GNPs) are graphite monolayers. It is a carbon allotrope composed of closely bonded carbon atoms organized in a hexagonal two-dimensional (2D) lattice. It is sp^2 hybridized, has an exceptionally thin nuclear thickness (0.345 nm), and a honeycomb structure with atomic carbon-carbon bonds length of 0.142 nm. Each carbon atom is bonded to three neighbor carbon atoms through **σ** bond and the remaining p electron from π bond with the surrounding atoms. The bonding between each carbon atom is very strong. Therefore, no misalignment and rearrangement between the carbon atoms when force is applied. Graphene is the strongest and thinnest nanomaterials (Yu *et al.* 2020). Single-layer graphene has a tensile resistance of 130 GPa, a Young's modulus of 1.0 TPa, and ten times the loading capacity of steel. Furthermore, it is one million times more conductive than copper (Abedi, Fangueiro, and Gomes Correia 2021). In graphite, graphene sheets are separated by 0.335 nm and are arranged on top of each other by weak van der Waals forces (Geim and Kim 2008). Carbon atoms have the same basic structural arrangement as graphite, fullerenes, and graphene, with six carbon atoms closely bonded in a hexagonal lattice separated by 0.142 nm. However, graphene represents the basic building block of graphitic materials with different dimensions as shown in Figure 1.2 (Geim and Kim 2008). As depicted, planar graphene sheets can be wrapped to form 0D fullerenes (C60), rolled to form 1D carbon nanotubes (CNT), or stacked to form 3D graphite. Graphene has attracted much attention of researchers over the last decades because of its superior mechanical, optical, and electrical properties which can be used widespread in biosensors, electronic devices, and composite materials. Due to the graphene's extraordinary characteristics, it’s been called as "super carbon."(Abedi *et al.* 2021).

1.2 Graphene Oxide

Graphene oxide (GO) has preference over graphene due to its easy processing, large-scale production, and low production cost. Recently, researchers have discovered the exceptional characteristic of GO materials which can be utilized as a catalyst active center for covalent/non covalent modification design. Also, the presence of oxygen-

containing groups enlarges the graphene's oxide interlayer gap. In contrast, graphene materials have some shortcomings such as easy agglomeration, low electrochemical activity, and difficult processing, which severely limit graphene's application. Thus, functional modification of graphene and graphene oxide is critical for broadening their applications. Many efforts have been put for the study of graphene and graphene oxide properties and synthesis process. It was concluded that the main difference is the presence oxygen bonded to carbon. Therefore, graphene oxide behaves as hydrophilic and easily dispersed in water, but graphene is naturally hydrophobic. GO has both aromatic sp^2 and aliphatic sp^3 domains which resulted in the enhancement of the interactions on its surface. GO can be reduced to G using a reducing agent but the obtained G has some structural defects which makes it inconsistence for mechanical and electronic applications (Georgakilas *et al.* 2016; Yu *et al.* 2020).

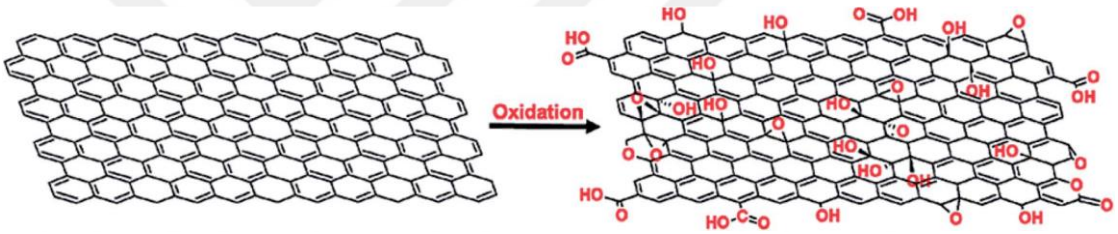

Figure 1.2 Oxidation of graphene sheet to form graphene oxide (Georgakilas *et al.* 2016)

1.2.1 Synthesize of graphene oxide

Graphite can be used as the raw material for GO synthesis. The GO obtained from graphite oxidation can be a conductor, semiconductor or insulator based on the oxidation degree which in turn affect the electrical and mechanical features. The band gap of graphene mainly depends on the oxygen concentration and thus, the band gap enhanced as the oxygen concentration increases and resulted in insulated GO (Ahmed *et al.* 2023). GO structure and properties will be affected by the synthesis method and the oxidation degree. GO was synthesized from graphite employing different methods such as Brodie, Staudenmaier, Hummers, and Marcon Tour. In 1859 Brodie discovered graphene oxide synthesis by oxidizing graphite material. Brodie was the pioneer of GO

synthesis, but it wasn't notices at that time. Brodie carried out this oxidation with potassium chlorate ($KClO_3$) and nitric acid (HNO_3) at 60 ^{O}C for three to four days. Brodie was able to investigate the elemental analysis of the prepared GO and revealed that the resulting product contains oxygen, carbon, and hydrogen (Thakur and Kandasubramanian 2019; Yu *et al.* 2016). 40 years later, Staudenmaier modified Brodie's method by changing the reagent to less risky such as sulfuric acid (H_2SO_4) to maintain acidic medium and attain good GO properties similar to Brodie's method (Farjadian *et al.* 2020). To enhance the oxidation rate and Brodie's method efficiency, the mixture was then diluted with $KClO_3$ and HNO_3.

In both the methods ClO_2, the explosive gas, is released to the environment and tend to explode in air. Hummer method utilized H_2SO_4 and HNO_3 for graphite treatment which led to less reaction time and preventing the formation of by- product ClO_2 gas which is advantageous for this method. Hummer and Offeman (Hummers and Offeman 1958) developed Hummer method by reacting the graphite with $KMnO_4$, $NaNO_3$, and concentrated H_2SO_4 to produce graphene oxide with similar oxidation degree to the previous methods. Hydrogen peroxide was then employed to remove $KMnO_4$ ions. Marcano and Tour modified Hummer's method by replacing sodium nitrate with phosphoric acid. Phosphoric acid is less harmful to the environment than sodium nitrate. It also collaborates with sulfuric acid and potassium permanganate to oxidize graphite. Although the prepared graphene oxide has a higher degree of oxidation and doesn't release any toxic gases using this method, it also requires a significant amount of concentrated sulfuric acid and $KMnO_4$, which raises the cost of processing raw materials and the disposal of waste liquids. The synthesis of GO occurs in two steps: oxidant insertion and sheet exfoliation as shown in Figure 1.3 (Yu *et al.* 2020).

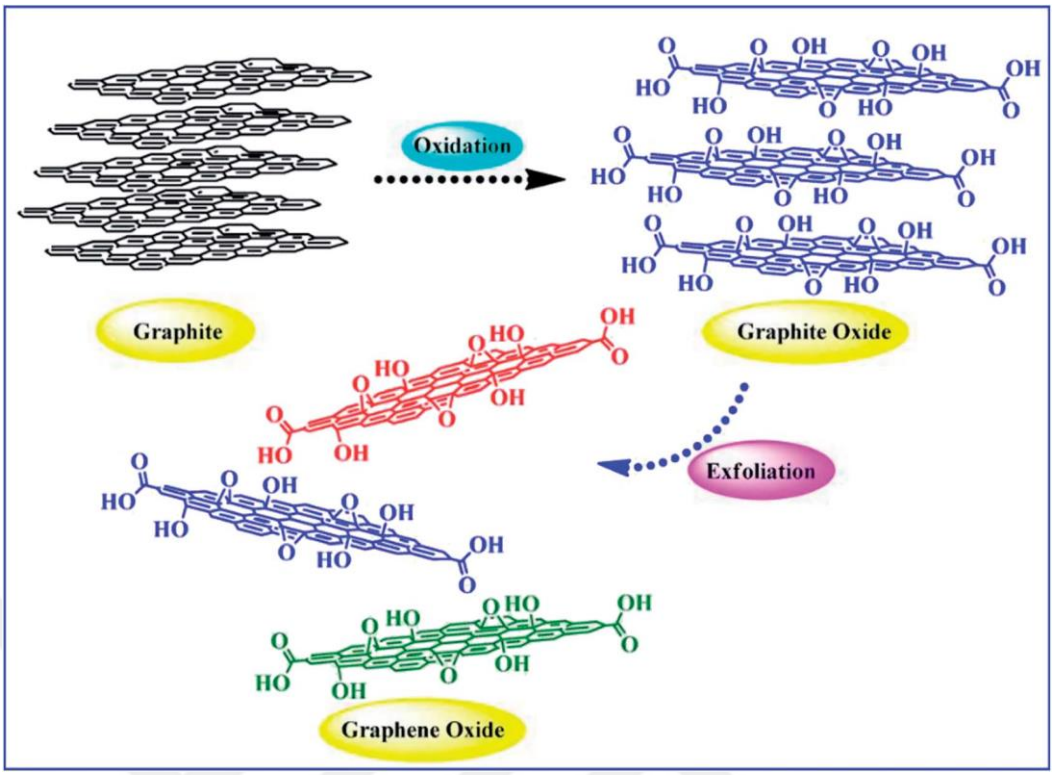

Figure 1.3 Graphene oxide preparation (Yu *et al.* 2020)

1.2.2 Structure of graphene oxide

Though many attempts have been performed by scientists such as Brodie, Hummer, Staudenmaier, Marcano and Tour, graphene oxide structure has not been verified yet. This is due to the amorphous nature of the obtained graphene oxide and lack of its stoichiometric atomic composition. GO is a non-stoichiometric chemical compound made up of carbon, oxygen, and hydrogen in varying ratios and this is significantly impacted by the processing techniques. During chemical exfoliation of GO, the introduction of oxygen into the graphene evidenced by oxygen epoxide groups (bridging oxygen atoms), carbonyl (C=O), hydroxyl (-OH), phenol, and even organosulfate groups (impurity of Sulfur). This means, oxygen is introduced into the graphene structure and resulted in lattice defects into on-plane functionalization defect and in-plane lattice defects. Therefore, superior features of GO were obtained from this defect which make it useful material from industrial perspective.

1.2.3 Characterization of graphene oxide

Graphene oxide characterization highlights its physiochemical features utilizing different techniques such as scanning electron microscopy (SEM) coupled with energy dispersive x-ray (EDX), Fourier transform infrared spectroscopy – attenuated total reflectance (FTIR-ATR), BET surface area, Zeta potential, particle size distribution using ZETA-SIZER equipment, and Raman spectroscopy.

1.2.3.1 Scanning electron microscope and energy dispersiv spektrum (SEM-EDS)

SEM- EDS analysis, is considered to be fast, cheap, and non-destructive approach to surface analysis technique. It is often utilized to survey surface analytical issues before proceeding to techniques that are more surface-sensitive and specialized. SEM-EDS is significant technique for obtaining the efficiency of graphene oxide oxidation process. SEM-EDS is well known technique for studying the surface analysis. Highly focused electron beam was used to produce high resolution images of surface topography. The sample can be enlarged as big as 20-50000 magnification with a resolution of about 5 nm. The electrons introduce to the sample surface with an energy 5-50 kV and produce significant amounts of secondary electrons which there intensity highly dependent on the surface topology. By measuring the intensity of the secondary electrons, an image of the sample surface is generated as a function of the scanning primary electron beam position. Using an energy of 1 kV of the primary electron beam would yields a high sensitivity (<5 nm) to topographic characteristics on the surface's outermost layer. Backscattered electrons and X-rays are another type of the electrons that yield from the primary electron bombardment. The backscattered electrons intensity gives information about the atomic number of the element in the sample which resulted in obtaining a qualitative elemental information. However, EDX or EDS analysis provides more quantitative elemental information (Abd Mutalib *et al.* 2017). Figure 1.4 shows the Picture of SEM/EDS equipment.

Figure 1.4 Picture of the SEM- EDS equipment

1.2.3.2 Fourier transform infrared spectroscopy – attenuated total reflectance (FTIR-ATR)

FTIR-ATR spectroscopy measures the chemical bonding interactions and the availability of functional group such as hydroxyl, carboxyl and epoxy groups which are very crucial in graphene oxide structure (Berthomieu and Hienerwadel 2009). Briefly, the samples are placed in contact with internal reflection elements (IREs) such as germanium or zinc selenide. Then the IR radiation is focused to penetrate the end of IRE and reflects down the IRE length. The IR radiation can penetrate from the IRE surface into the sample for up to ~1μm. The absorption of radiation is regarded to the basic background vibrations of chemical bonding while the radiation reflection gives indication of the presence or absence of functional group and materials chemical structure. The results obtained from FTIR can be represented in the term of absorbance or transmittance (y-axis) and the radiation wavelength (x-axis) in the range 4000-400 cm wavelength (mid-infrared region). The penetration depth of ATR-FTIR corresponds to the wavelength of IR light, which ranges from few hundred nanometers to more than

1 m (Berthomieu and Hienerwadel 2009). Therefore, ATR-FTIR is not a sensitive surface investigation technique for nanomaterials with dimensions in the tens of nanometers. Figure 1.5 shows the ATR-FTIR equipment picture.

Figure 1.5 ATR-FTIR analyzer device picture

1.2.3.3 BET (Brunauer-Emmett-Teller) surface area

N_2-physisorption is a high-quality tool for determining the materials texture, surface area, pore volume and diameter, and pore size distribution. Physisorption occurs when the adsorptive gas (e.g. N_2) brought into contact with the solid surface (adsorbent) at 77 K. Prior the experiment, the sample is degassed to remove any impurity or pre-adsorbed gas as shown in Figure 1.6. The intermolecular forces are like that in charge of the imperfection of actual gases and the condensation of vapors. Moreover, special molecular interactions such as polarization, field-dipole, field gradient quadrupole are typically originated from the specific geometric and electrical features of the adsorbent and the adsorptive. In terms of porous adsorbents, surface area can be categorized into two types: external surface area which is related to the area outside the pore while internal surface area corresponding to the surface of the whole pore walls (Keshavarz *et*

al. 2022). According to IUPAC, pore texture can be classified into three categories (Rahman *et al.* 2021):

1- Pore widths which are less than 2 nm called micropores.
2- Pore widths between 2-50 nm are called mesopores.
3- Pore widths exceed 50 nm are called macropores.

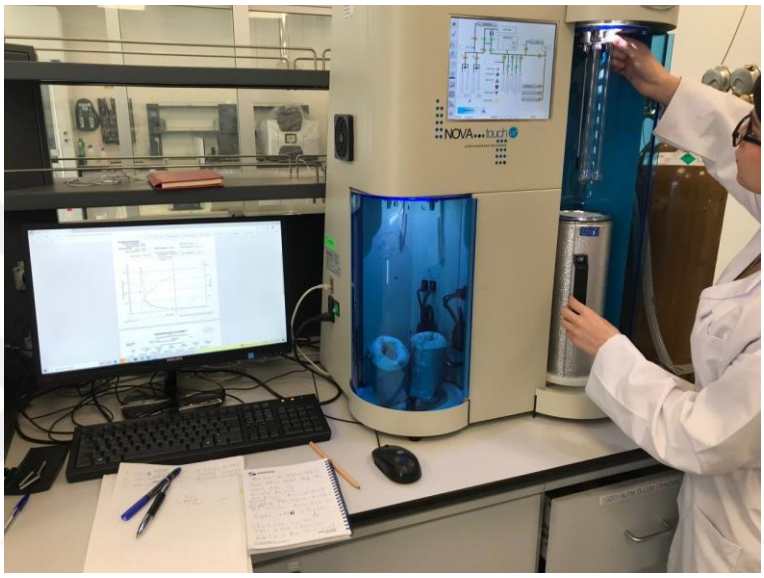

Figure 1.6 The BET-Surface Area device in picture

1.2.3.4 Zeta potential and partical size distribution

Zeta potential (ZP) is an analytical technique that deals with the obtaining of surface charge of nanoparticles in colloidal solution. The surface of a charged particle attracts a thin layer of opposite charge and strongly attached to it, yielding a thin liquid layer called the Stern layer; when the particle diffuses in solution will be engaged by an outer diffuse layer that composes of freely related ions, which resulted in the creation of electrical double layer. ZP can be obtained through velocity measurement of the charged particles migrating toward the electrode across the sample solution in the existence of outer electric field. The range of ZP values is between +100 to -100 mV and its magnitude is an indication of the colloidal stability. Normally, nanoparticles with ZP values higher than +30 mV or lower than -30 mV indicates high stability.

Lower ZP values resulted in coagulation, aggregation, or flocculation because of van der Waals interparticle forces (Shnoudeh *et al.* 2019). Figure 1.7 is shown Zeta Potential properties for nano fluidics.

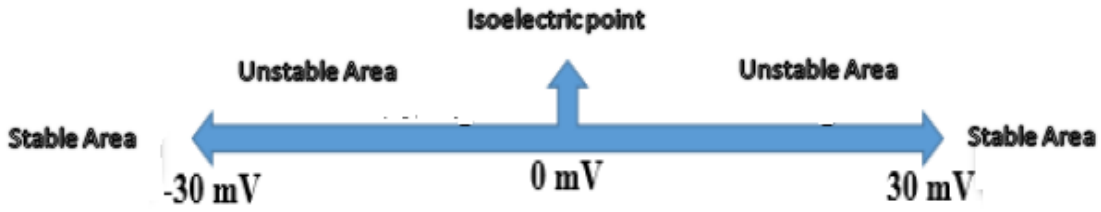

Figure 1.7 The zeta potential for nano fluidics

Generally, the physical properties (mechanical, optical, electrical, etc.) of a material at macro dimensions generally differ significantly from the nano-size region when the particle sizes are smaller than 100 nanometers. Materials that are insoluble at the macroscale can become soluble at the nanoscale, and vice versa for opaque materials. These examples can be multiplied much more. One nanometer is one billionth of a meter, and the typical range of application for nanotechnology is 1 to 100 nm. Examining this image will allow one to get a sense of how different sized materials are distributed. The device picture used for the zeta potential and particle size distribution analyses is shown in Figure 1.8.

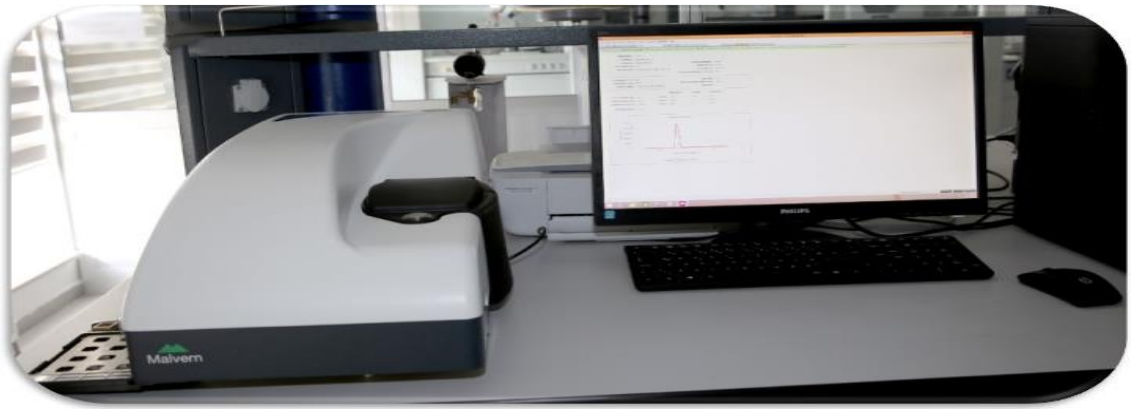

Figure 1.8 Picture of the zeta potential and particle size distribution device

1.2.3.5 Raman spectroscopy

Raman spectroscopy is a powerful analytical technique widely used for characterizing materials, including graphene oxide. It employs a highly focused laser beam to interact with molecular vibrations, generating unique spectral information. This technique is particularly effective in analyzing the structure and quality of graphene-based materials. The D/G ratio in Raman spectroscopy is a critical parameter for graphene oxide. It refers to the intensity ratio of the D-band (around 1350 cm^{-1}, indicating defects or disorders in the carbon lattice) to the G-band (around 1580 cm^{-1}, associated with the vibration of sp^2-bonded carbon atoms in a 2D hexagonal lattice). This ratio is used to assess the degree of disorder or defects in graphene structures, with a higher D/G ratio indicating more defects (Chaloupková *et al.* 2023).

Figure 1.9 Raman spectroscopy device picture

1.2.4 Graphene oxide properties

The most desirable attribute of GO is its ability to be (partially) reduced to sheets resembling graphene by removing oxygen-containing groups and recovering a conjugated structure. Reduced grapheme oxide sheets are typically regarded as one type of chemically generated graphene. rGO has also been referred to as functionalized graphene, chemically modified graphene, chemically converted graphene, or reduced graphene. GO has attracted much attention of researchers due its excellent features such as high hydrophilic characteristic, able to form stable aqueous colloids to facilitate the assembly of macroscopic structures using simple and cheap solution processes, produced by utilizing cheap graphite as feedstock with inexpensive chemical process with a high yield (Farjadian *et al.* 2020). Graphene sheet composes trigonally bonded sp^2 carbon atoms and is ideally flat (Thakur and Kandasubramanian 2019). The GO sheets are composed of sp^3 carbon atoms that are tetrahedrally linked and slightly shifted above or below the graphene plane. GO sheets are rough due to the structural deformation and the presence of covalently bound functional groups. Graphene's conductivity is mostly dependent on the long-range conjugated network of the graphitic lattice. Functionalization disrupts the conjugated structure and localizes p-electrons, reducing both carrier mobility and carrier concentration. Even though GO contains conjugated regions, the lack of percolating routes between sp^2 carbon clusters prevents classical carrier transport over extended distances (>μm). Consequently, as-synthesized GO sheets or films are typically insulating, with a sheet resistance of at least 10^{12} Ω/sq. The bonded groups and lattice imperfections alter the electronic structure of graphene and serve as strong scattering centers that influence the electrical transport. Therefore, the reduction of GO is not only concerned with removing the oxygen-containing groups linked to the graphene and other atomic-scale lattice defects, but also with restoring the conjugated network of the graphitic lattice. These structural modifications restore graphene's electrical conductivity and other features. Optical properties is a good observation for depicting the modification in GO structure before and after reduction. Since a reduction process can greatly improve the electrical conductivity of GO, the increased concentration and mobility of charge carriers will result in a brown color and semi-transparency. The reduction in a colloid state by chemical reduction, such as

hydrazine reduction, typically results in a black precipitation from the original yellow–brown suspension. This is likely due to an increase in the hydrophobicity of the material, which improves the reflection of incident light, giving rGO films a metallic luster compared to their GO film precursors (Habte and Ayele 2019).

1.2.5 Application of graphene oxide

Since graphene oxide has a remarkable physical and chemical features, it has many applications in different areas such as energy, environment, green chemistry, catalysis, photocatalytic, nanodevices, bioimaging, biomedicine, and electronics (Song *et al.* 2020; Thakur and Kandasubramanian 2019). Also, GO has some biological applications on laboratory scale as in antibacterial coatings, drug delivery, photo-thermal cancer thermal, neural stem cells, and selective differentiation of mesenchymal. In addition, GO can be utilized in the environmental sector in the area of adsorption and water purification, solar desalination, and environmental sensing. Moreover, GO has also used in the field of energy storage (Jia *et al.* 2022). The utilization of nanoparticles in various applications is strongly affected by plenty factors such as size, shape, surface area, number of facets, facet order, etc. In many applications, the utilization of nanoparticles necessitates immobilization on a substrate surface and thus GO can act as a substrate for nanoparticles in many applications especially when conductivity or anchoring sites is beneficial. Although GO has many applications in different areas, there is still few in the field of biomedicine. Thus, hybrid materials composed of carbon dots with GO would be a promising material soon.

1.3 Boron

Boron with a symbol B is unique as it is the only nonmetal in Group 13 (IIIA) of the periodic table. B has atomic number 5 and atomic mass 10.81 and thus shares some similarities with carbon and silicon. B has a density of 2.84 g/cm^3 and melting point of 2550 ^{o} and considered to be a semiconductor between conductors and non-conductors elements (Brdar-Jokanović 2020). Boron electronic distribution is 1 s^2 $2s^2$ 2p with three electron valences. Boron has the ability to form planar univalent compounds, BX_3,

when X= alkyls, halides, etc., making 120º bonding angles. The empty *p* orbital makes theses compounds electron-pair acceptors or Lewis acids. Two types of boron isotope presents naturally ^{10}B and ^{11}B with a ratio of ~20% and ~80% respectively. The presence of boron isotopes reflects variety of boron naturally deposits such as high ^{10}B ore in Türkiye and low ^{10}B ore in California Other types of boron isotopes are available naturally such as ^{8}B, ^{12}B, and ^{13}B with low half-lives of <1 s. Boron ranks 51st of the most common element available in the earth's crust with a concentration 3 g per metric ton. ^{10}B isotope is one of the vital feedstock in industry with its capability to make a wide variety of compounds employing nuclear materials and power plants, with a greater thermal neutron holding capacity than the other isotope (Mermer and Şengül 2020).

Though boron element is not available freely in nature, the artificially produced boron mineral exists in two forms as amorphous and crystalline. Amorphous boron is in the form of blackish or brown powder, and the crystalline boron element is black in color, hard and brittle Boron is known as the hardest and highest electro-positive element among nonmetals after diamond. When exposed to infrared light, boron becomes transparent to certain wavelengths. In addition, while it has low electrical conductivity at temperatures under normal conditions, it has a semiconducting feature because it is highly conductive at high temperatures (Brdar-Jokanović 2020).

1.3.1 Boron deposits and reserve quantities in Türkiye and the world

Boron ore is not found in all parts of the world, but it is concentrated in certain regions and countries. There are boron minerals in approximately 10 countries around the world. Countries with significant boron reserves; Türkiye, USA, China, and Russia. According to 2017 Boren data, the distribution of world boron reserves on the basis of $\%B_2O_3$ is given in Table 1.1. Since the world boron reserves vary according to the data of the countries, it is very difficult to say the world boron reserve amount clearly and reliably. In this case, it shows once again the strategic importance of boron in the world (Sokmen and Buyukakinci 2018).

Boron reserves in the world, especially in Türkiye, Russia and the USA have 1.2 billion tons of reserves. It is seen that 70 million of them are in Russia and 80 million tons and 6.2% in the USA. Considering the amount of boron reserves and consumption in the world, it is estimated that there are enough boron minerals for the world for hundreds of years (Sokmen and Buyukakinci 2018)

Table 1.1 Distribution of world boron reserves on the basis of $\%B_2O_3$ (Sokmen and Buyukakinci 2018)

COUNTRY	**TOTAL RESERVE (Thousand tons of B_2O_3)**	**TOTAL RESERVE ($\%B_2O_3$)**
Türkiye	953	72.8
Russia	100	7.6
USA	80	6.1
Chili	41	3.6
China	47	3.1
Peru	24	1.8
Serbia	22	1.7
Bolivia	19	1.5
Kazakhstan	15	1.1
Argentina	9	0.7
Total	1310	100

About 86% of the boron in the world is utilized in four major areas: ceramics, glass, fertilizer, and detergents. As shown in Figure 1.10. 48% is utilized in the glass, 15% in the agriculture, 15% in the ceramic, 3% in the detergent, and the remaining 19% in other sections. However, in Türkiye 28% of boron is utilized in glass, 34% in the detergent, 21% in the ceramic, 4% in agriculture, and 13% for other applications (Elevli *et al.* 2022).

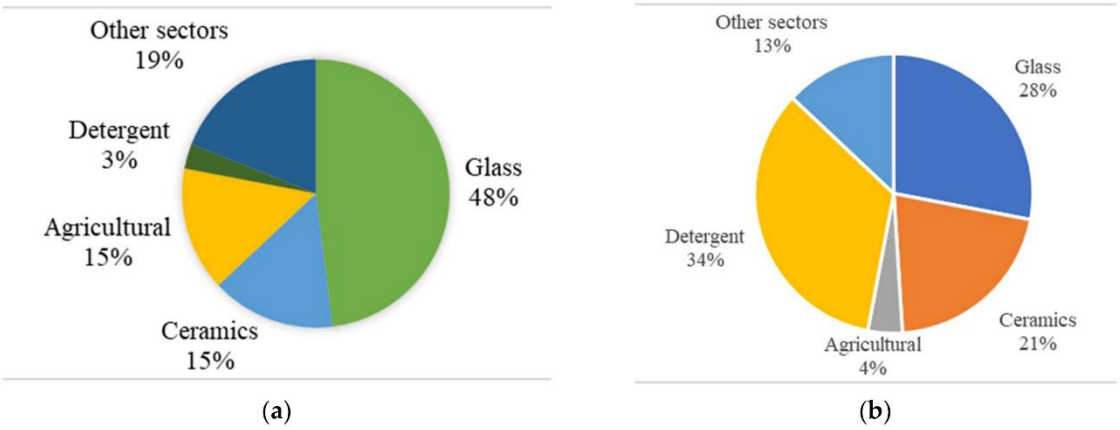

Figure 1.10 (a) Usage of boron in the world and (b) Usage of boron in Türkiye (Elevli *et al.* 2022)

Türkiye is considered as a rich country in terms of mining resources such as boron, chromium, trona, and marble. Around 72% of the total boron deposits in the world (See Table 1.1) are available in Türkiye. The most important boron minerals that Türkiye owns are tincal, colemanite, and ulexite. Türkiye is considered to be the second highest producer of boron after the USA. 8% of its boron minerals is utilized locally, and 92% is exported outside Türkiye (Kar, Şen, and Demirbaş 2006).

Borate deposits known in Türkiye are located in the south of the Sea of Marmara, in the Western Anatolia region and within an area of 300 km in the east-west direction and approximately 150 km in the north-south direction, in Kırka/Eskişehir, Bigadiç/Balıkesir, Kestelek/Bursa and Emet/Kütahya. It is located in 4 regions. In this country, tincal ($Na_2O.2B_2O_3.10H_2O$) and colemanite ore ($2CaO.3B_2O_3.5H_2O$) come first in terms of reserve amount. The most important tincal deposits in Kırka region, located in the southwest of our country, colemanite deposits and ulexite mineral in Emet and Bigadiç regions are found in very low amounts in Bigadiç, and occasionally together with colemanite ore in Kestelek region (Elevli *et al.* 2022).

The large amount of boron reserves in Türkiye provides advantages in terms of production. Boron ore in Türkiye is extracted in large deposits and by open pit methods.

In addition, the enrichment of boron ore is carried out. The data of the reserve amounts on the basis of minerals are shown in Table 1.2.

Table 1.2 Türkiye's boron reserves (Boren 2020)

Area	Ore type	Total (TON)
EMET	Ulexite -Probertite - Colemanite	1.811.072.520
KIRKA	Tincal	824.720.950
BIGADIC	Colemanite, Ulexite	628.350.480
KESTELEK	Colemanite	5.254.920
	Total	3.269.398.870

1.3.2 Boron compounds

Boron minerals are natural compounds containing various proportions of boron oxide (B_2O_3) in its structure. Although it is classified by considering sodium, magnesium, calcium and crystal water content in its structure, a systematic classification could not be made because the crystal system of many boron minerals is not known exactly. More than 230 boron ores are available naturally, and those with commercial value are pandermite, tincal, ulexite, colemanite and kernite. In Türkiye, the most common minerals are tincal as sodium source, colemanite as calcium source, and ulexite as sodium and calcium source. These most common minerals and ores are enriched in boron (concentrated boron) by applying physical methods, and then refined to obtain various boron chemicals (Turkbay *et al.* 2022).

1.3.3 Boric acid (H_3BO_3)

Boric acid is a hydrate form of boric oxide and presents in the form of trihydrate, orthoboric acid (B_2O_3. $3H_2O$ or H_3BO_3), and as a monohydrate, metaboric acid (B_2O_3. $3H_2O$ or HBO_2). The orthoboric type-boric acid is the only one has been considered to be with a commercial value and usually referred as boric acid. Boric acid (orthoboric acid) is a white, shiny, odorless mineral that can crystallize as hexagonal leaflets. It is a boron mineral with a molecular weight of 61.84 g/mol, a B_2O_3 content of 56.4%, a

density of 1.5272 g/cm^3, a heat of formation of 1095.3 kJ/mol and a heat of dissolution of +22.2 kJ/mol. It is an acid that is slightly soluble in cold water and highly soluble in hot water and can be entrained with water vapor (Tolun 1981).

The solubility of boric acid in water between 0°C and 100°C is shown in Figure 1.11. As the temperature increasing, the solubility of boric acid increases significantly. In boric acid formation solution, barium, lithium, strontium, and generally calcium-containing salts greatly increase the apparent ionization constant of boric acid. Therefore, it significantly increases the solubility of boric acid in aqueous media at room temperature Boric acid production from colemanite ore in industry is obtained by cooling solutions containing 17-18.01% concentrated H_3BO_3 prepared at approximately 90°C to 35 to 45°C (Çelikoyan 2008).

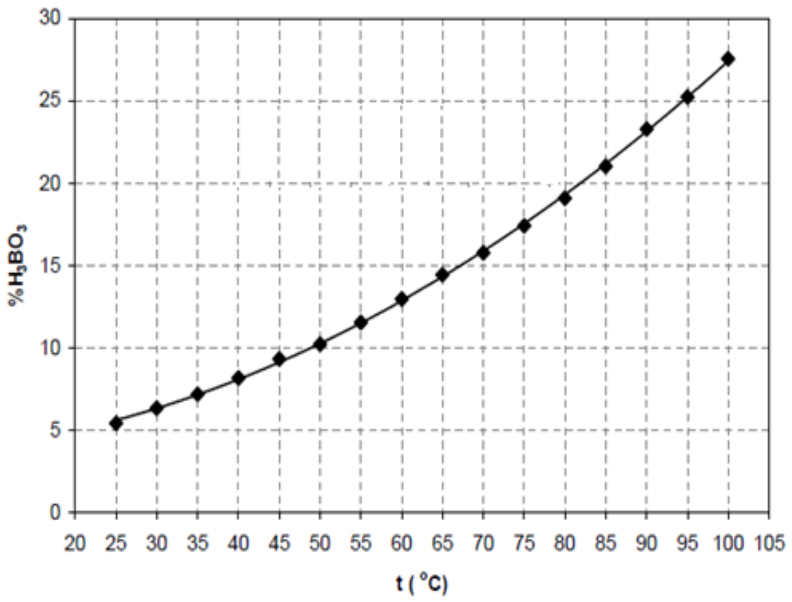

Figure 1.11 Solubility curve of crystals of boric acid in pure water (Çelikoyan 2008)

The presence of salts such as KCl, Na_2SO_4 and K_2SO_4 in boric acid production solutions increases its solubility gradually, but as it is known that the solubility decreases with the presence of mineral acids and salts such as NaCl, LiCl. By adding borax to solutions, polyborates are formed (Tolun 1981). When boric acid is heated slowly, it loses its

water in its structure and turns into metaboric acid. Metaboric acid has three distinct crystal structures.

Orthorhombic metaboric acid (HBO_2- III. melting point: 176 °C)

Monoclinic metaboric acid (HBO – II. melting point: 200 °C)

Cubic Metaboric Acid (HBO_2- I. melting point: 236 °C)

Boric acid, which has been utilized in many industrial sectors, is produced in Türkiye and in various regions of the world. boric acid: It is used in many sectors from nuclear systems, boron alloys, fire retardants, nylon, antiseptics, glass, textile, glass fiber, enamel to fertilizer industry. Boric acid is produced mostly from colemanite ore in the world (Mumcu 2010).

1.3.4 Other boron compounds

Borax pentahydrate (Sodium tetraborate pentahydrate $Na_2B_4O_7.5H_2O$) is a boron compound, also called rhombohedral crystalline tincalconite in basic medium. It is known that in fully formed structures, there is 5 moles of crystal water, not exactly 5 moles, and it has the chemical formula $Na_2B_4O_{7.}5H_2O$. X-Ray diffraction analysis of borax pentahydrate shows that it has the chemical formula $Na_2B_2O_7OH_2.5H_2O$. After the tincal mineral dissolves in water, borax pentahydrate crystals are produced by keeping the temperature constant at 60-65°C during crystallization. Borax pentahydrate transforms to borax dihydrate structure at temperatures of 160-170˚C, to borax monohydrate structure at temperatures of 190-300˚C, and to anhydrous borax form at temperatures of 400-500˚C (Erkan 2002; İnal 2009).

Borax exists in nature as tincal ($Na_2B_4O_7.10H_2O$) and tincalconite ($Na_2O.2B_2O_3.5H_2O$). Borax production is generally made from tincal in Türkiye. Refined borax is obtained from calcium-structured borates such as kernite, tincal, ulexite, colemanite and

pandermite, or from borax-containing lake waters. Concentrated tincal ore, approximately 10 mm in size, is fed into the reactor with hot water at about 100°C and is easily dissolved at this temperature. Since the clays in the tincal structure are generally colloidal in nature, they are precipitated with the help of a suitable precipitator and separated from the suspension. The part that leaves this solution is called slime. The solution containing borax is passed through a filter press and sent to the crystallizer via conveyor belts. Borax, which is crystallized in the crystallizer at 40°C, is taken from the system to contain 5% moisture with a centrifuge system and stored at 60°C after drying.

Anhydrous borax ($Na_2B_4O_7$), which is a sodium borate phase, exists in different crystalline and glassy structures indicated by the chemical formula $Na_2B_4O_7$. It is formed by calcining borax and melting it in melting furnaces at 980°C. When the molten borax mineral reaches the appropriate fluidity, it is taken from the furnace and anhydrous borax in amorphous structure is obtained by means of water-cooled drums. Anhydrous borax glasses dissolve more slowly in water than hydrates (Turkbay *et al.* 2022).

Another borate compound is sodium perborate ($NaBO_2.H_2O_2.3H_2O$). To prepare sodium perborate, borax and NaOH solutions are heated with water vapor in the reactor to obtain sodium metaborate solution. After the solution obtained and filtered, it is cooled by flowing air counter currently. The sodium metaborate stored in the tanks is sent to the crystallizer, which is constantly fed 70% H_2O_2. Sodium perborate ($NaBO_2.H_2O_2.3H_2O$) formed because of the reaction accumulates at the bottom of the crystallizer. Obtained sodium perborate crystals are removed from the mother solution by centrifugation. The resulting moist crystals are dehumidified by a fluidized bed dryer. It is an active oxygen source containing 10.3% oxygen in its sodium perborate structure.

1.3.5 Toxicity of boric acid

Although boric acid (H_3BO_3) are utilized in laundry detergents, cleaning agents, and fertilizers, it has some toxicological inhalation concern and skin toxicity. Most of the

toxicity of boron comes from boric acid based on the literature (Hadrup, Frederiksen, and Sharma 2021). Boric acid has been well known as a reproductive toxicant for at least the past 20 years. The studies by Weir and Fisher in 1972 established boric acid as toxic to the male reproductive system, the skin, and growth inhibitor(Chapin and Ku 1994) . In one study on rats with the inhalation of cellulose with 20% boric acid presented decline of foetal body weight. After oral and dermal exposure, boric acid has some fatal and other toxicity endpoints were activated. In another study, 113 workers were exposed to boric acid and boron oxide dust with an average 4.1 mg particulate dust/m^3. Compared with 214 workers as an experiment control, it was found that more symptoms of eye irritation, dryness of the nose, throat, mouth, sore throat, and cough. Concerning intact skin, it was observed that the skin absorbs 0.2% of the boric acid exposing dose with flux 0.009 μg/cm^2. Also, some fatalities happened after boric acid ointment exposing to human skin. Moreover, acute toxicity with fatalities after boric acid ingestion for instance 5 of 11 infants were accidentally poisoning and died after ingesting infant formulae prepared from a bottle of "distilled" water that accidently contained 2.5% boric acid (Hadrup *et al.* 2021).

1.3.6 Boric acid production

There are some feedstocks for boric acid production as ulexite and HCl, tincal and H_2SO_4, colemanite and H_2SO_4, tincal and HNO_3.Durıng World War I (WWI), boric acid was prepared from ulexite mineral and HCl. After that, due to the high cost of HCI (two fold) sulfuric acid was used instead (Demirel *et al.* 2015).

Boric acid is produced from borates and minerals. Thus, they react with sulfuric acid to generate boric acid. The greatest source of borates in the world is a California boron mine. Sodium borax can be reacted with an inorganic acid such as sulfuric acid or hydrochloric acid to form boric acid. To generate boric acid using sulfuric acid, sodium borohydride is first introduced to the reaction tank, followed by the slow addition of dilute sulfuric acid until the solution is substantially acidified and its pH approaches zero. This results in the formation of a saturated solution of borax or ortho-borate. Then, the hot solution crystallizes and cools in vacuum. Crystals of boric acid will then

develop. Separate the crystals from the solution and cool the residual solution until sodium sulfate is produced. In the subsequent phase, boiling water is used to extract boric acid, which is then refined and packaged for sale. The reactions for the production of boric acid with sulfuric acid from tincal and colemanite are given below.

$$2CaO_3B_2O_3.5H_2O + H_2SO_4 + 3H_2O \rightarrow 6H_3BO_3 + 2\ CaSO_4.2H_2O$$

$$Na_2B_4O_7.10H_2O + H_2SO_4 \rightarrow 4H_3BO_3 + Na_2SO_4 + 5H_2O$$

The manufacture of boric acid from tincal with sulfuric acid yielded 95 percent pure boric acid. Raffi nation might raise the purity to 99.95 percent. Türkiye's ETI Mine General Directorate was the first to employ boric acid produced from colemanite with H_2SO_4 in the industrial sector. Nonetheless, this procedure is more expensive and requires more energy (Demirel *et al.* 2015).

1.4 Experimental Design

1.4.1 Taguchi method

Experimental design was determined by British statistician Ronald Fisher's research and research on agriculture in the early 1920s. This method was used intensively only in the agricultural sector in the United States, to determine the effects of various fertilizers and climatic conditions on different products, as well as agriculture. While the basics of experimental design were not known until the early 1950s, it was very much in use in Japan. Japanese engineers worked on these methods and experimental design methods (turns into statistics) were more effective than American engineers.

Later, Japanese scientist Genichi Taguchi brought a new approach to this method in the 1980s and developed a product and process design method that would not be affected by environmental conditions, had low variation, and was suitable for the intended

purpose. It has been widely used in quality control stages, in the design of a new product for the road, and in research and development studies (Canıyılmaz 2001).

According to the Taguchi method, the first step to ensure quality characterization is the experimental design sequence made before the targeted product production. The main goal of the Taguchi method is; The controllable factors that have the change in the determined target value should be determined, and the uncontrollable factors are the determination of the most appropriate process steps to be minimum (Şimsek 2014).

To summarize Taguchi method in working conditions,

1-In a competitive economic process, it is necessary to continuously improve the quality characteristics of the enterprises and to reduce the costs and to maintain the continuity of the enterprises. For this reason, targeted studies should be continuous in order to keep the continuous quality improvement and costs at a minimum level (Patel *et al.* 2021).

2- The quality of the targeted product is the loss that may occur due to the quality and cost of this product in the market. The loss that a product may cause in the consumer due to its quality characteristic increases in proportion to the square of the deviation (Wang *et al.* 2020).

3- The final quality and economic cost of the target product are determined by considering the design and production process of the product. Market research, design and process development, and processes in the production process at the first stage of the design and production of the product. There is also a control mechanism called Offline and On-line Quality Control. On-line inspection covers the quality activities during the production of the final product and at the next stage of production. Offline, on the other hand, is of great importance for the final product, which is aimed to reduce the undesired situations in the final product in the design process (Lin *et al.* 2020).

4- In order to reduce undesirable situations in the final product, the irregular effects that affect the quality of the product should be controlled. Experiments designed within the framework of experimental designs are used to minimize the performance variability of the product or process (Şimsek 2014).

It is necessary to design a systematic quality engineering in order to obtain appropriate results in a product or process of the Taguchi method. This allows both the experimental design to be easily understood and the targeted results to be understandable. We can explain the basic application steps of the Taguchi method under 7 headings (Şimsek 2014).

- Identifying and expressing the problem
- Determining the factor levels to be evaluated
- Determination of the appropriate orthogonal sequence
- Assigning factors or interactions to columns
- Conducting the experiments
- Statistical calculations and evaluation
- Conducting validation experiments (Şimsek 2014).

After determining the purpose for the realization of the process, the factors to be evaluated are determined. Taguchi method, It divides the factors into two, expressed as controllable signal and uncontrollable noise factor. Experimental design is determined according to the number and levels of controllable factors (Özkurt 1999).

5- The characteristics of many performance criteria for the developed design model are taken into consideration when choosing performance statistics. To enable data analysis, it is crucial to ascertain the performance statistic's target value. The S/N ratio is the performance statistic value selected in Taguchi designs, and it is used to evaluate the effectiveness of the design's outcomes. Known as the signal to noise ratio (S/N) or Taguchi loss function, there are three distinct target-appropriate functions. Thus, the following formulas are used to compute S/N ratios, using "small best," "largest best,"

and "nominal best" as the desired outcomes (Bademlioglu, Canbolat, and Kaynakli 2020).

Where lowest (small) is best;

$$SN_S = -10\ Log\left(\frac{1}{n}\sum_{n=1}^{n} y_i^2\right) \quad (1,1)$$

Where the highest (large) is the best;

$$SN_L = -10\ Log\left(\frac{1}{n}\sum_{n=1}^{n} \frac{1}{y_i^2}\right) \quad (1,2)$$

Where nominal is at best;

$$SN = -10Log\left(\frac{\tilde{y}^2}{S^2}\right) \quad (1,3)$$

Competent in Equations: Experimental i: the experiment's result value; n: the number of trial repetitions the test result's mean; and S^2: an expression of the test result's variance.

2. LITERATURE REVIEW

2.1 Synthesis of Graphene Oxide

Muzyka et al studied the oxidation degrees of graphene oxide with modified Hummers Method using sulfuric acid, nitric acid, sodium nitrate, sodium dichromate and potassium permanganate. It was concluded that the degree of oxidation with sodium dichromate was lower than that of others. It was found that the best oxidation was achieved when the chemicals in the current Hummers Method were used in excess proportions (Muzyka *et al.* 2017).

In another study which include graphene oxide synthesis by Hummer's method, it was examined that the effect of particle size and reaction time were tested. 6, 18 and 25 nm of particle size were investigated and it was observed that the oxidation time depends on the particle size and shape of the graphite. The reaction time was found as 1-2 days when 6 and 18 nm of particle size of graphite used. This reaction time sharply decreased (2 hours) when 25 nm flake graphite used (Shojaeenezhad *et al.* 2017).

Mendonca et al studied for examining the formation mechanisms and of graphene oxide synthesis to understand the interaction between graphene layers and sulfate species. They mentioned that during the long reaction time of graphene oxide synthesis, manganese and nitrate ions protect the sulfate ions. It was concluded that the presence of sulfate ions played an important role in the formation of oxygenated functional groups in the structure (Mendonca *et al.* 2018).

Korkmaz and Kariper studied the synthesis, properties, and supercapacitor applications of graphene and graphene oxide-based aerogels. The article highlights the high potential of graphene-based materials in energy storage technology and emphasizes the importance of three-dimensional (3D) structures developed with these materials in the production and application of energy storage devices (Korkmaz and Kariper 2020).

Bentedlaouti et al studied a novel, scalable, and cost-effective synthesis method for graphene oxide (GO) and reduced graphene oxide (rGO) without using chemical reducing agents. The key focus of the research is on enhancing the physicochemical and biological properties of these materials by decorating them with silver nanoparticles (AgNPs). This innovative approach results in the production of GO and rGO with high thermal stability and significant antioxidant and antimicrobial properties. The synthesized GO and rGO, along with their silver nanoparticle-decorated variants (GO-Ag and rGO-Ag), were thoroughly characterized and tested for their biological activities. The study found that the presence of AgNPs significantly enhances the antioxidant activity of the graphene-based materials. This enhancement is attributed to a synergistic effect between the silver nanoparticles and the graphene nanomaterials. The results indicated a substantial antibacterial effect, with rGO-Ag showing the highest efficacy. This enhanced antibacterial activity is likely due to a combination of the physical disruption caused by the sharp edges of the reduced nano-walls and efficient charge transfer between the bacteria and the graphene material (Bentedlaouti *et al.* 2024).

Fardinpour et al studied the green synthesis of graphene oxide/copper oxide (GO/CuO) nanocomposites using ginger essential oil (GEO). This innovative approach aimed to enhance the antibacterial properties of the nanocomposites. The key findings of the study are centered around the successful synthesis of these nanocomposites and their effective antibacterial activity against both gram-positive (Staphylococcus aureus) and gram-negative (Escherichia coli) bacteria. The results demonstrated that the GO/CuO-GEO nanocomposite exhibited notably high antibacterial activity, surpassing that of the GO/CuO nanocomposite and even some standard antibiotics in certain cases. This enhanced activity is attributed to the synergistic effect of the graphene oxide, copper oxide, and ginger essential oil components in the nanocomposite (Fardinpour *et al.* 2024).

Kumar *et al.* studied efficient electrochemical synthesis of highly oxidized graphene oxide (GO) for enhanced energy and environmental applications. The research focuses on a novel one-pot two-step process for synthesizing GO, which involves the exfoliation

of graphene sheets from an anodic graphite electrode in a sulfuric acid-phosphoric acid mixture, followed by oxidation using platinum-coated titanium electrodes and potassium permanganate as the oxidizing agent. A variety of techniques such as XRD, Raman, TGA, FESEM, TEM, FT-IR, XPS, and Boehm's titration were employed for thorough characterization of the synthesized GO. The results indicated successful production of GO with high thermal stability and efficient removal capabilities for organic pollutants like methylene blue, rhodamine B, and methyl orange dyes from aqueous solutions (Kumar *et al.* 2023).

Nayak *et al.* synthesized reduced graphene oxide (ACrGO) using the aqueous extract of Araucaria Cunninghame resin as a sustainable catalyst for the photodegradation of methylene blue (MB) dye. The research emphasizes the green synthesis approach and its effectiveness in enhancing the catalytic properties of graphene oxide. The synthesized ACrGO nanocomposite demonstrated superior catalytic activity in degrading MB dye, achieving an impressive 84% degradation in just 50 minutes under sunlight exposure. This high efficiency is attributed to the enhanced surface area and charge transfer properties of ACrGO, making it a potent catalyst for dye degradation (Nayak *et al.* 2024).

Muniyalaksi *et al.* studied synthesis of graphene oxide (GO) nanosheets. The core of the study is the modified Hummer's method used to produce GO nanosheets, involving graphite powder, sulfuric acid, and potassium permanganate. The results are analyzed through X-Ray diffraction, Raman spectroscopy, FTIR spectroscopy, and scanning electron microscopy, each providing insights into the structural and chemical properties of the GO nanosheets. The study concludes by affirming the successful synthesis of GO nanosheets, highlighting their distinct physical characteristics and potential applications in various fields (Muniyalakshmi *et al.* 2020).

In another study, non-plastic, and glycerol-plasticized chitosan-reduced graphene oxide nanocomposites were synthesized via chemical reduction of graphene oxide layers with environmentally friendly L-ascorbic acid. In the study, it was tried to find the best conditions for the synthesis of reduced graphene oxide with L-Ascorbic acid. The effect

of glycerol on the structure and the thermal-mechanical and electrical properties of chitosan-graphene nanocomposites were evaluated. The interaction between the reduced graphene oxide sheets distributed homogeneously along the chitosan surface was observed. While a decrease in crystallinity values was observed in non-plastic chitosan nanocomposites under oxidative atmospheric conditions, an improvement in their mechanical properties and thermal stability were observed. The combined use of glycerol and reduced graphene oxide greatly improved the mechanical properties. As the amount of reduced graphene oxide was increased, the electrical conductivity value of the nanocomposite increased. This study was conducted to improve the performance properties of chitosan-reduced graphene oxide nanocomposite (Cobos *et al.* 2018).

2.2 Boron Removal Studies

Boron is normally present in ground water and sea water, is a vital micronutrient for plants, but is also toxic in excessive amounts. However, high boron concentration is detected in seawater at around 5 ppm (T. Chen *et al.* 2020), and in some groundwater, the concentration can reach up to 119 pp (Guo *et al.* 2013). In these regards, separation of high concentration of boron from water is urgently demanded. In literature there have been many separation techniques which eliminate the excessive boron from water such as coagulation/flocculation, sedimentation, filtration, adsorption (Kamcev *et al.* 2019), membrane technology (Lan *et al.* 2021), ion-exchange (Wang *et al.* 2021), electrocoagulation (Chen *et al.* 2020).

Electrodialysis, and hybrid processes have been studied. Among them, adsorption is the most promising method because it has flexible and easy operation and does not generate waste or toxic sludge (Ipekci *et al.* 2020).

İpekçi *et al.* synthesized heterogeneous ion exchange membranes for separation and recovery of boron and lithium from aqueous solution. After applying the optimum process conditions, it was found that 59 % boron recovery was achieved in acid and base cells (Ipekci *et al.* 2020).

Chen et al studied boron removal with electrocoagulation method. They found that 50% of the Boron was removed from the river (spiked with 10 mg/L of B) in 2 h with a 0.2 A current; and 80% of the Boron was removed from produced water (spiked with 50 mg/L B) in 2 h with a 1.0 A current (M. Chen *et al.* 2020).

2.3 Boron Adsorption Studies

Adsorption can be accepted as a superior technique for removal of boron from water. Many adsorption materials have been developed, aiming for high adsorption capacity, fast uptake rate, having low cost, and high renderability.

Taşçı *et al.* prepared Chitosan/functionalized-SWCNT-COOH by the impregnation method. Under the experimental conditions of 91.17 mg/L of boric acid concentration, pH of 5.86, and 76.17 min, the optimal adsorption capacity was reported as 62.06 mg/g (Taşçı *et al.* 2022).

Chen et al synthesized mesoporous silica (MCM-41) and pyrocatechol@MCM-41 by sol-gel method. The specific surface area of pyrocatechol@MCM-41 reached 362 m^2/g and the abundance of pyrocatechol was 1.29 mmol/g the Langmuir adsorption capacity was reported as 17.7 mg B/L (Chen *et al.* 2019).

Tang et al studied with silica material as an adsorbent for efficient removal of boron from wastewater. They focused on increment of hydrophilicity of adsorbent matrix and developed a material which helps boric acid can be access to the pores easily. And they concluded that 80 % of boron removal was achieved within 3 minutes (Tang *et al.* 2017).

Al-Afy and Sereshti studied adsorption removal of boron from water with Fe_3O_4 doped Graphene oxide. The Langmuir adsorption capacity of Fe_3O_4 doped Graphene oxide was found as 35.7 mg-B/L. And they concluded that due to the magnetic effect of the

adsorbent, adsorbent can be separate easily for reuse 10 times without any specific deterioration (Al-Afya and Sereshtia 2019).

Chen et al doped nitrogen in graphene oxide and investigated the effect of addition of positive charges in GO sheets on boron removal. They found that the adsorption capacity was found as twenty times higher than that of graphene oxide (Chen *et al.* 2017).

Although there have been many applications of metal organic frameworks (MOFs) in adsorptive removal of many pollutants, there have been a few literatures on adsorption of boron on MOFs. Lyu et al studied to synthesizing of different metal organic framework such as ZIF-8, UiO – 66, MIL-96 (Al), MIL-100 (Fe), MIL-100 (Cr), MIL-53(Cr) and MIL-101(Cr) as adsorbent for boron removal from wastewater. ZIF-8 showed most effective performance with an adsorption capacity of 191 mg/g (Lyu *et al.* 2017).There have been a few studies on Graphene oxide-based materials for boron adsorption in literature. Table 2.1 shows the studies on boron removal by graphene oxide-based materials.

Table 2.1 Studies on boron removal by graphene oxide based materials

Adsorbent	Adsorption capacity (mg/g)	Isotherm constant (L/mg), (Langmuir)	Conditions	References
Nitrogen doped graphene oxide	58.70	0.00409	Adsorbent dose: 1.6 g/L; T: 25 ^{O}C; pH: 8.5; Operating time: 48 h; Initial boron concentration: 5 mg L^{-1}	(F. Chen *et al.* 2017)
GO/ZIF-67 Graphene oxide / metal organic framework composite	66.65	0.0112	Adsorbent dose: 1.0 g L^{-1}; T: 25 ^{O}C; pH > 10; Operating time: 400 min; Initial boron concentration: 200 mg L^{-1}	(Hu *et al.* 2020)
Magnetic graphene oxide nanocomposite	35.70	N/A	Adsorbent dose: 2.7^{3} g/L; T: 25 ^{O}C; pH: 9.2; Operating time: 14.8 min; Initial boron concentration: 100 mg/L	(Al-Afy and Sereshti, 2019)

3. MATERIALS AND METHODS

3.1 Materials

In this thesis, for controlling the reaction temperature in the experimental systems, a POLYSCIENCE 15-R circulating water bath was used. For stirring processes, an IKA C-MAG-HS7 magnetic stirrer and a M TOPS-Ms3040 mechanical stirrer were employed. The drying process was carried out using a DAIHAN vacuum oven (WOV-70) and a JSR atmospheric oven (Jsof-250). Additionally, the water requirement for all processes was met by a Merck Millipore Essential 10 device, which produces water according to Type 2 standards.

In the study, the characterization of graphene oxide materials was conducted at Çankiri Karatekin University Central Research Laboratory using Quanta chrome - Nova Touch LX4 for BET analysis, Bruker–Tensor 2 for FTIR analysis, Carl Zeiss-Sigma 300 VP for SEM+EDS analysis, and Malvern - Zetasizer Nano ZS for Zeta Potential and Particle Size Distribution analysis. The RAMAN spectroscopy analysis was carried out at Çukurova University Central Research Laboratory using Renishaw - In Via Qontor.

For the synthesis of graphene oxide using the Staudenmaier, Staudenmaier-Hummers, and Hummer's methods, chemicals such as natural graphite (50 μm), HNO_3, H_3PO_4, H_2SO_4, $KClO_3$, $KMnO_4$, H_2O_2 and HCl have been used. Boric acid was used for boron removal. In all methods, chemicals of analytical purity were preferred for procurement.

3.2 Experimental Method

In this thesis work, graphene oxide has been synthesized using the Staudenmaier, Staudenmaier-Hummers, and Modified Hummers methods. Graphene oxide samples synthesized by different methods were taken in varying amounts according to the $L_9(3^4)$ experimental design model and used in different concentrations of Boric Acid and

different pH environments. The aim was to optimize the quality criteria of graphene oxide and the removal of boric acid using the Taguchi method.

3.2.1 Synthesis of graphene oxide from graphite using the Staudenmaier method

In the synthesis of graphene oxide from graphite using the Staudenmaier method, 15 g of graphite was added to a double-walled glass reactor along with 75 mL of nitric acid (70%) and 225 mL of sulfuric acid (98%) and the reaction temperature was set to 5 ºC. Subsequently, 150 g of potassium chlorate (99%) was slowly added to the reactor. The mixture was stirred with a magnetic stirrer at 5 ºC for 24 hours, and then the reaction temperature was raised to 95 ºC and stirred for an additional 6 hours. To remove metal ions from the mixture, 5 mL of hydrochloric acid (37%) was added, and the reaction was terminated. The washing and purification process was carried out by the settling method with the addition of 200 mL of pure water until the pH reached approximately 2-3. After the washing process, the GO mixture was finally dried in an oven at 50 ºC to obtain graphene oxide. Figure 3.1 provides the flow diagram for the synthesis of graphene oxide by the Staudenmaier method.

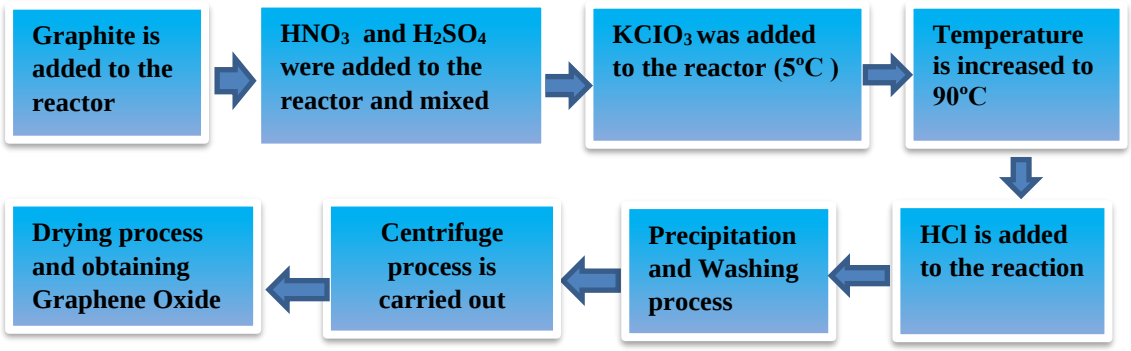

Figure 3.1 Flow diagram of graphene oxide synthesis by the Staudenmaier method

3.2.2 Synthesis of graphene oxide from graphite using the Staudenmaier-Hummers method

In this method, a different approach from the literature has been adopted, aiming to introduce a new approach by combining the Staudenmaier and Hummers methods for the synthesis of graphene oxide from graphite. With this goal, 15 g of graphite was added to a double-walled glass reactor along with 225 mL of nitric acid (70%), 225 mL of sulfuric acid (98%), and 15 mL of phosphoric acid (85%), and the reaction temperature was set to 5 ºC. Subsequently, 100 g of potassium chlorate (99%) and 30 g of potassium permanganate (99%) were slowly added to the reactor. The mixture was stirred with a magnetic stirrer at 5 ºC for 24 hours, and then the reaction temperature was raised to 95 ºC and stirred for an additional 6 hours. To remove metal ions from the mixture, 5 mL of hydrochloric acid (37%) was added, and the reaction was terminated. The washing and purification process was carried out by the settling method with the addition of 200 mL of pure water until the pH reached approximately 2-3. After the washing process, the GO mixture was finally dried in an oven at 50 ºC to obtain graphene oxide. Figure 3.2 provides the flow diagram for the synthesis of graphene oxide by the Staudenmaier-Hummers method.

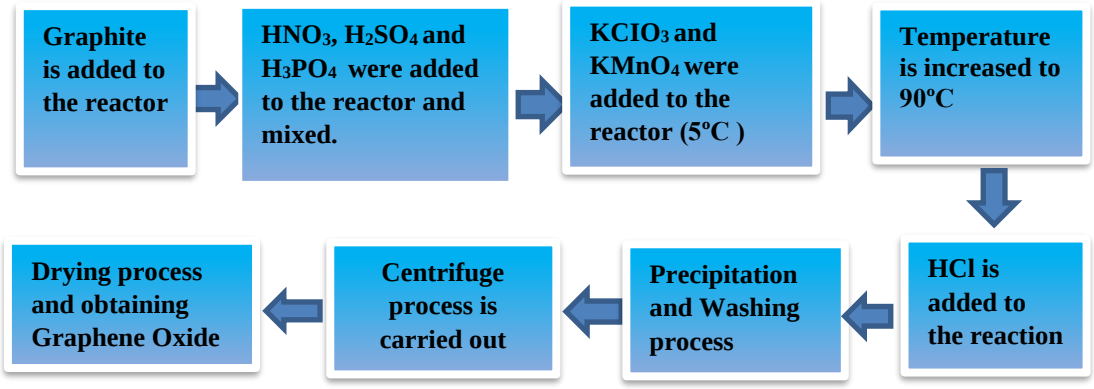

Figure 3.2 Flow diagram of Staudenmaier – Hummers method graphene oxide synthesis

3.2.3 Synthesis of GO (Graphene Oxide) from graphite using the modified Hummers method

In the synthesis of graphene oxide from graphite by the Hummers method, 15 g of graphite was added to a double-walled glass reactor containing 300 mL of sulfuric acid (98%) and 15 mL of phosphoric acid (85%), and the reaction temperature was set to 5 ºC. Subsequently, 45 g of potassium permanganate (99%) was slowly added to the reactor. The mixture was stirred with a magnetic stirrer at 5 ºC for 24 hours, and then the reaction temperature was raised to 95 ºC and stirred for an additional 6 hours. To remove metal ions from the mixture, 5 mL of hydrochloric acid (37%) was added, and the reaction was terminated. The washing and purification process was carried out by the settling method with the addition of 200 mL of pure water until the pH reached approximately 2-3. After the washing process, the GO mixture was finally dried in an oven at 50ºC to obtain graphene oxide. Figure 3.3 provides the flow diagram for the synthesis of graphene oxide by the Modified Hummers method.

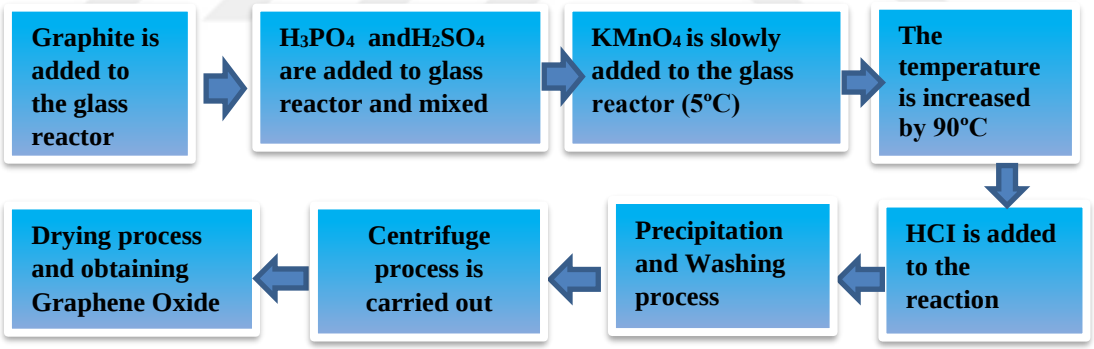

Figure 3.3 Flow diagram of graphene oxide synthesis by the Modified Hummers method

3.3 Experimental Method

In this study, the objectives and goals were initially determined. In the subsequent stage, quality characteristics related to these objectives and goals were identified. From the experimental design models, the most suitable model for the study, the $L_9(3^4)$ model consisting of 4 parameters and 3 levels, was selected. The parameters and their levels have been determined. The quality characteristics results of the designs have been

analyzed by the Taguchi optimization method using the Minitab software. Optimum levels for the parameters have been determined based on the analysis results.

3.3.1 Determination of the optimum characteristics of the L_9 (3^4) experimental design

For the optimization experiments of boric acid removal with graphene oxide samples, an L_9 (3^4) orthogonal experimental design plan consisting of 4 parameters and 3 levels has been selected. The parameters and their levels are given in Table 3.1, while the coded and uncoded levels related to the quality criteria of the L_9 (3^4) orthogonal experimental design plan are provided in Table 3.2.

Table 3.1 Parameters and levels of the $L_9(3^4)$ experimental design

	Symbol	Parameters	Levels		
			1	**2**	**3**
Parameters and Levels	A	pH	3,5	7	10
	B	Graphene Oxide Type	Staudenmaier	Staudenmaier-Hummers	Hummers
	C	Graphene Oxide amount (g)	1	2	3
	D	Concentration of Boric acid	0,1g/100ml	0,5g/100ml	1g/100ml

Table 3.2 Coded and uncoded data of the $L_9(3^4)$ experimental design

Experiment No.	Coded Levels				Uncoded Levels			
	A	**B**	**C**	**D**	**A**	**B**	**C**	**D**
GO1	1	1	1	1	3,5	Staudenmaier	1g	0,1g/100ml
GO2	1	2	2	2	3,5	Staudenmaier-Hummers	2g	0,5g/100ml
GO3	1	3	3	3	3,5	Hummers	3g	1 g/100ml
GO4	2	1	2	3	7	Staudenmaier	2g	1 g/100ml
GO5	2	2	3	1	7	Staudenmaier-Hummers	3g	0,1g/100ml
GO6	2	3	1	2	7	Hummers	1g	0,5g/100ml
GO7	3	1	3	2	10	Staudenmaier	3g	0,5g/100ml
GO8	3	2	1	3	10	Staudenmaier-Hummers	1g	1g/100ml
GO9	3	3	2	1	10	Hummers	2g	0,1g/100ml

3.3.1.1 The determined quality characteristics of the experimental design of L_9 (3^4)

In the study of optimization of boric acid removal with graphene oxide samples, quality characteristics were selected for the graphene oxide (GO) samples obtained after boron removal, and optimization studies were conducted based on the results of these selected criteria. The determined quality criteria are given below:

- The first quality criterion is based on the D peak at 1350 cm^{-1} and the G peak at 1585 cm^{-1} in Raman analysis. An increase in the ratio of the D/G peak is considered an indicator of increased irregularity, and thus a decrease in the number of layers. Therefore, for GO synthesis, a low intensity of the D/G peak is desired, as it indicates fewer defects in the structure.

- The second quality criterion is the atomic ratio of carbon to oxygen (C:O) determined by Scanning Electron Microscopy – Energy Dispersiv Spektrum Method (SEM-EDS), selected in terms of the degree of oxidation. For GO, a strong oxidation is desired, so this ratio is preferred to be low.

- The third and fourth quality criteria are measured with ZETA-SIZER. In these measurements, particle size distribution analysis (nm) and zeta potential measurement (mV) were conducted in GO dispersions to improve stability. In GO characterization, small values of particle size and zeta potential are preferred.

- The surface area (m^2/g) of the GO was measured using the BET device as the seventh quality criterion. The objective was to obtain a high surface area measurement result for the GO. The desired value in surface area analysis, measured in square meters per gram (m^2/g), is the highest possible. The increased surface area has a beneficial impact on the rate of mass transfer, capacity for adsorption, size of micropores, and size of lamellae.

- The sixth and final quality criterion is the amount of boric acid adsorbed per gram of graphene oxide. For the calculation of boric acid removal, boric acid analysis was conducted using a titration method with normality known sodium hydroxide solution and mannitol indicator in the solutions. A mass-balance relationship, the following equation was used to calculate (equation 3.1) the amount of adsorbate adsorbed onto the adsorbents in various conditions:

$$q_t = (C_0 - C_t)\frac{V}{W} \quad (3.1)$$

where C_0 and C_t (mg/L) are the liquid phase concentrations of the adsorbate at time = 0 and t, respectively. V (L) is the volume of the adsorbate solution and W (g) is the weight of the adsorbents used. It is aimed to achieve a high amount of boric acid adsorbed per gram grapheme oxide.

Explanations for the quality criteria given above related to the optimization study are provided in Table 3.3. Figure 3.4 presents the flow diagram for the $L_9(3^4)$ Experimental design.

Table 3.3 Determined quality criteria and weights

Quality Criteria	Symbol	Explanation	Information	The goal for GO
1	ID/IG	The Ratio of the D Peak to the Intensity of the G Peak	Defective in structure	Smaller is better
2	C/O	Carbon-Oxygen Ratio	Degree of oxidation	Smaller is better
3	PS	Particle Size	Feature improvement	Smaller is better
4	ZP	Zeta Potential	Stable distribution	Smaller is better
5	BET	Surface Area	Degree of porosity	Larger is better
6	H_3BO_3	Boric Acid Removal	Graphene Oxide Boric Acid Adsorption Capacity	Larger is better

Figure 3.4 The proposed performance assessment scheme of the experimental design

4. EXPERIMENTAL RESULTS

In this section of the study, the effects of environmental pH, initial graphene oxide amount, type of graphene oxide, and boric acid concentration on graphene oxide samples were investigated and interpreted following the L_9 (3^4) experimental design.

4.1 Interpretation of Graphs and Images of Graphene Oxide Samples Following the L_9 (3^4) Experimental Design

In Figure 4.1, FTIR graphs of graphene oxide samples synthesized by Graphite (Grpht), Staudenmaier (GO-S), Staudenmaier-Hummers (GO-SH), and Hummers (GO-H) methods are presented. The vibration and deformation peaks of O-H groups formed in the structure of graphene oxide are observed at 3391 cm^{-1} and 1410 cm^{-1}, the C=O vibration peak at 1721 cm^{-1}, the C-O stretching vibration peak at 1221 cm^{-1}, and the C-O tension peak at 1046 cm^{-1}. FT-IR analyses have shown that graphene oxide samples synthesized by different methods (GO-S, GO-SH, GO-H) have been successful. Figure 4.2 shows the FTIR analysis results to analyze the changes in the structure of graphene oxide samples following the L_9 (3^4) experimental design. FTIR analysis results indicate that, the functional groups in the structure of the graphene oxide samples remained intact and retained the properties of graphene oxide, after the removal of boric acid. The graphs also clearly show that as the experiment number increases, the intensity and breadth of the peaks of 3391 cm^{-1} and 1721 cm^{-1} related to the presence of OH groups in graphene oxide samples under high pH conditions increase.

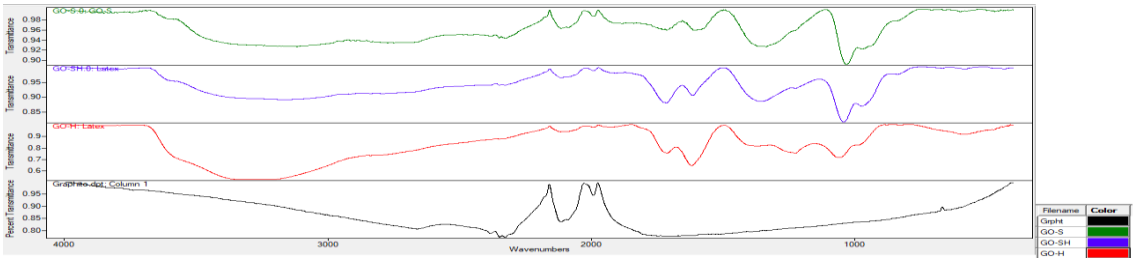

Figure 4.1 FTIR graphs of graphene oxide samples synthesized from graphite by oxidation methods

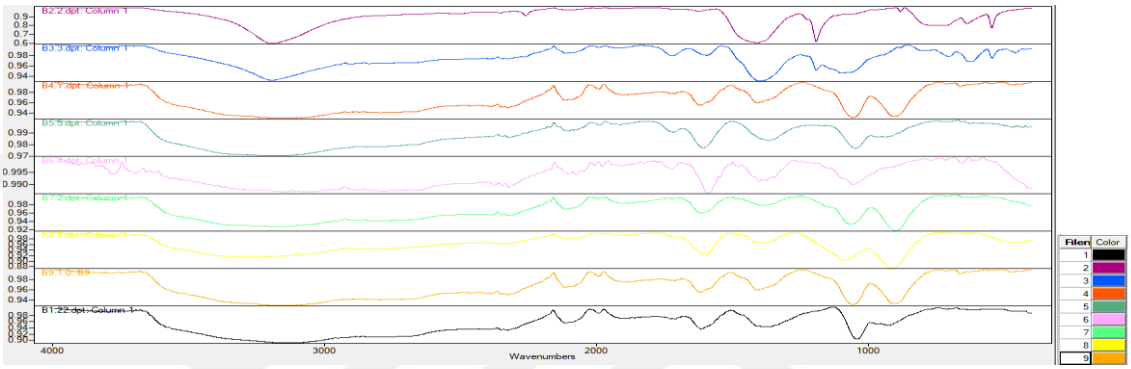

Figure 4.2 FTIR graphs of graphene oxide samples at the end of the L_9 (3^4) experimental design

Figure 4.3 shows RAMAN graphs of graphene oxide samples synthesized from Graphite (Grpht) via Staudenmaier (GO-S), Staudenmaier-Hummers (GO-SH) and Hummers (GO-H) methods. In graphene oxide samples, it is observed that the G peak, which is not inherent in the structure of graphite, is formed and the intensity and width of the D peak increases. This shows that the synthesis of graphene oxide from graphite was successful for their methods.

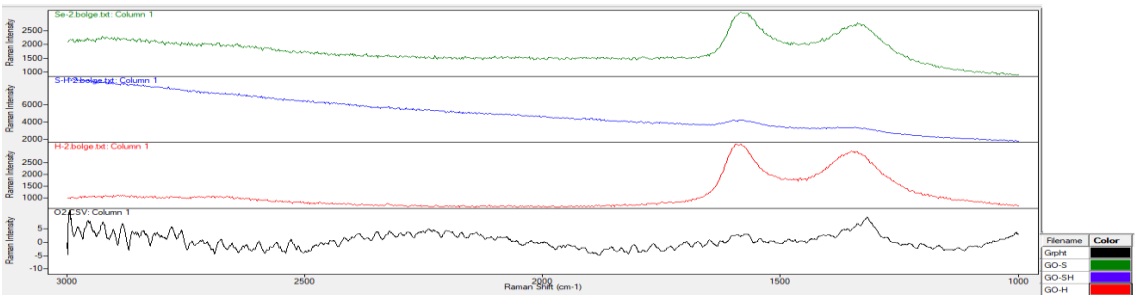

Figure 4.3 Raman graphs of graphene oxide samples synthesized from graphite by oxidation methods

When the Raman graphs of graphene oxide samples at the end of the L_9 (3^4) experimental design are examined (see Figure 4.4), D peak at 1350 cm^{-1} and G peaks at 1585 cm^{-1} are seen in the Raman pattern. The shift of the G peak to smaller wavelengths is considered indicative of an increase in aggregation and the number of layers, and the increase in the intensity ratio (ID/IG) of the D and G peaks after reduction indicates an increase in disorder and consequently a decrease in the number of layers. In this thesis, the Raman analysis patterns of the synthesized GOs, as shown in Figure 4.4, reveal that the G peaks have shifted to wavelengths greater than 1585. This suggests that the synthesized GOs are of a multilayered structure.

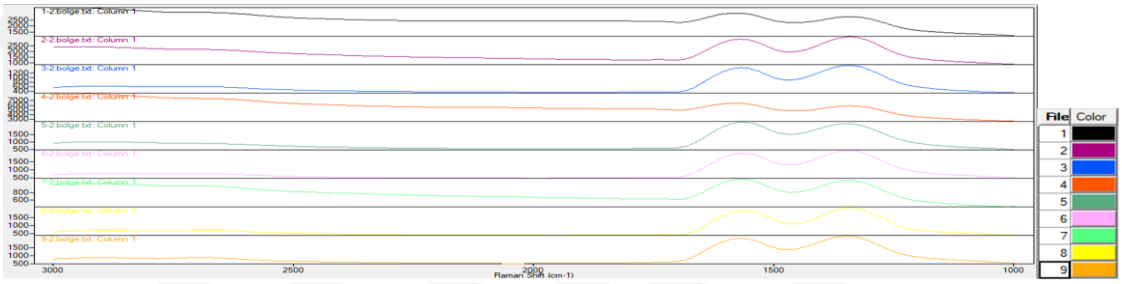

Figure 4.4 Raman graphs of graphene oxide samples after appying the L_9 (3^4) experimental design

For single-layer graphene, the D band, which is inactive, becomes active in chemically prepared graphene in the overlapping products of the drying steps. The ratio of the D and G bands (ID/IG) is a measure of the disorder in the structure. Additionally, the D band provides information about defects and imperfections in the layers of graphite, graphene oxide, and graphene structures. The G band characterizes the arrangement of carbon atoms in sp^2 hybridization in bulk. In Figure 4.5, SEM and EDS analyses of graphene oxide samples synthesized by different methods (GO-S, GO-SH, GO-H) are presented. Upon examining the EDS results, a decrease in the C:O ratio compared to graphite is observed, which can be considered an indicator of the functional groups attached to the structure.

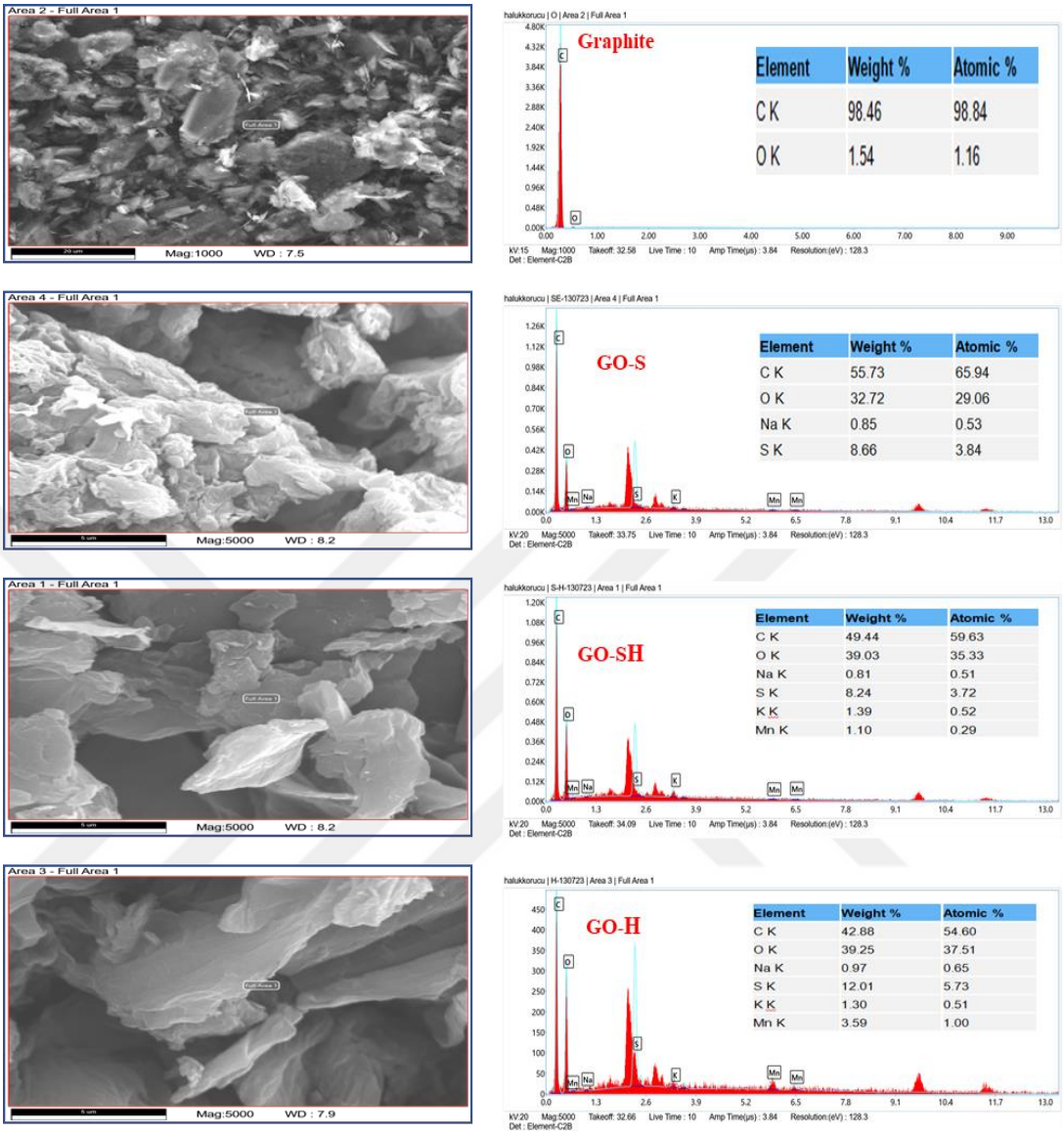

Figure 4.5 SEM-EDX images of graphene oxide samples synthesized from graphite by oxidation

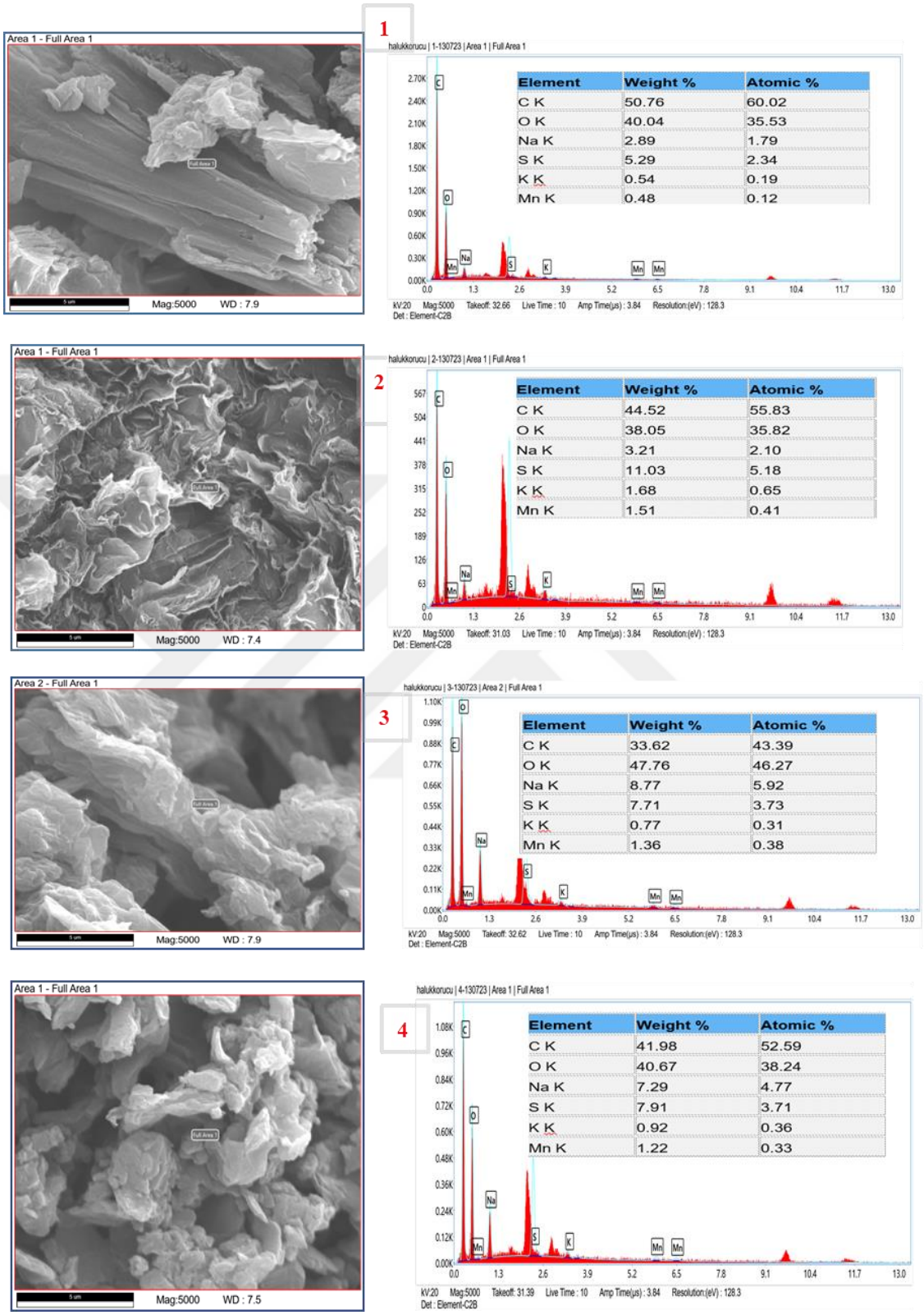

Figure 4.6 SEM-EDX images (1-4) of graphene oxide samples following the L_9 (3^4) experimental design

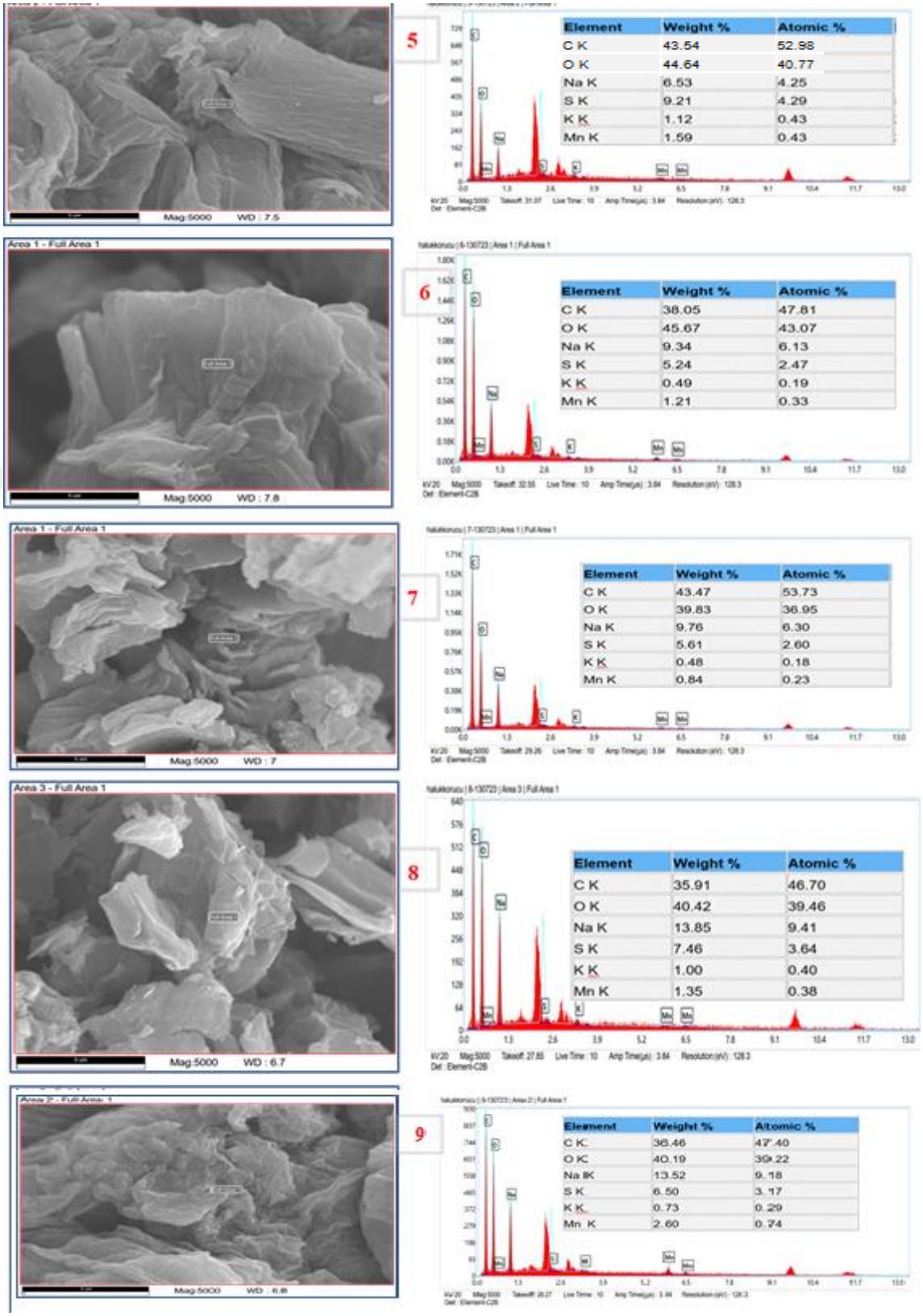

Figure 4.6 SEM-EDX images (5-9) of graphene oxide samples following the L_9 (3^4) experimental design (Continued)

When the SEM images of the graphene oxide synthesis in Figure 4.6 are examined, it is observed that they are consistent with the literature. When the EDX analysis data in Table 4.1 are examined, a decrease in the C:O ratios is observed after applying the L_9 (3^4) experimental design. The decrease in the C:O ratio can be attributed to the increase in the degree of oxidation due to the increase in the number of functional groups forming bonds with carbon, as a result of the addition of boric acid to the environment and NaOH added to adjust the pH.

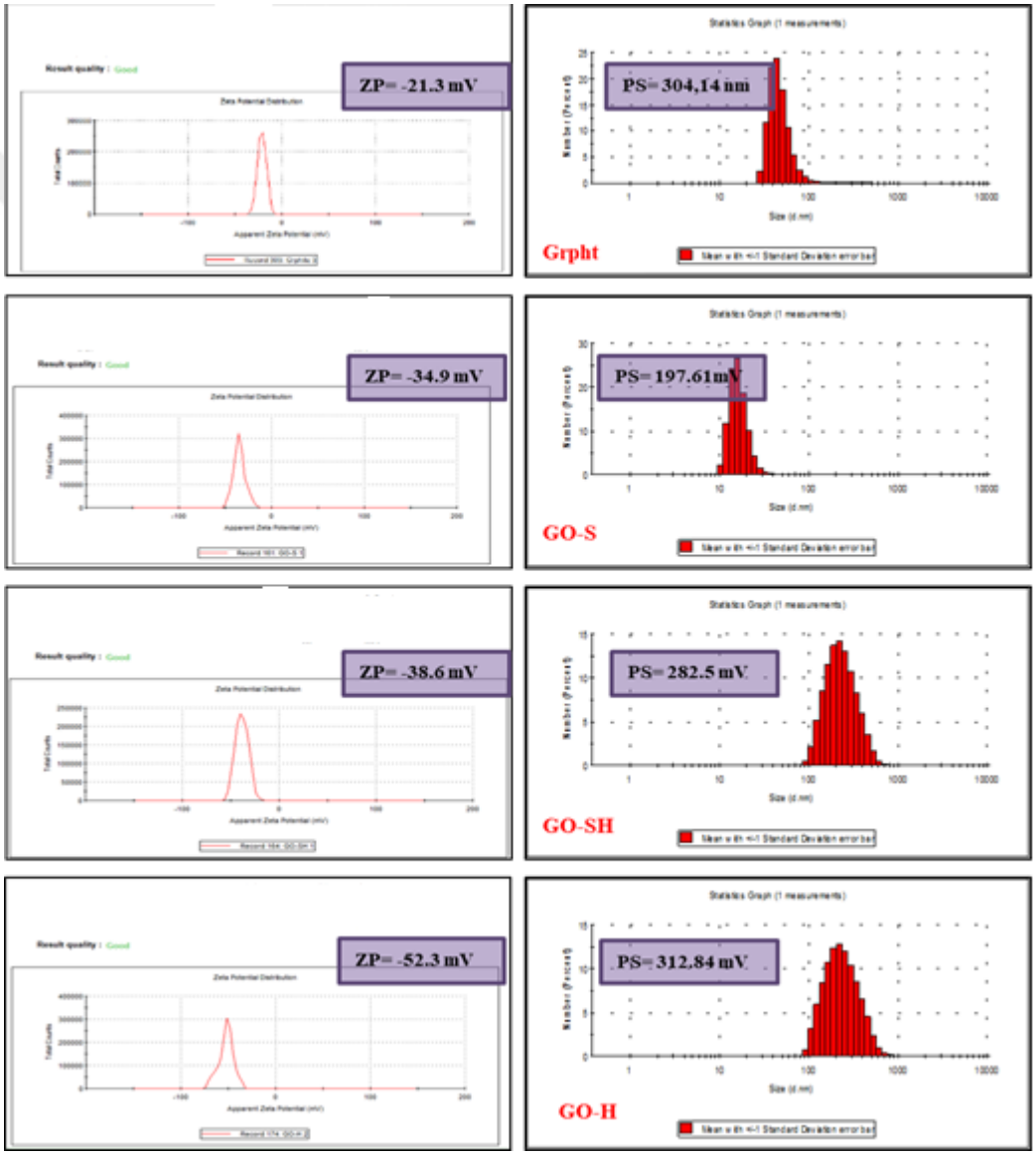

Figure 4.7 ZETA-SIZER Spectra of graphene oxide samples synthesized by oxidation methods from graphite

Figure 4.7 presents the Zeta Potential and Particle Size results for Graphene Oxide samples synthesized from graphite using oxidation methods. It is observed that the Zeta Potential values are high for graphite value, and decrease progressively towards the Staudenmaier, Staudenmaier-Hummers, and Hummer's methods, respectively. This indicates that the dispersion property of the Hummers method is better. In terms of Particle Size values, the best result is obtained with the Staudenmaier method. It is seen that the number of nano-sized particles in the Staudenmaier method is better compared to other methods.

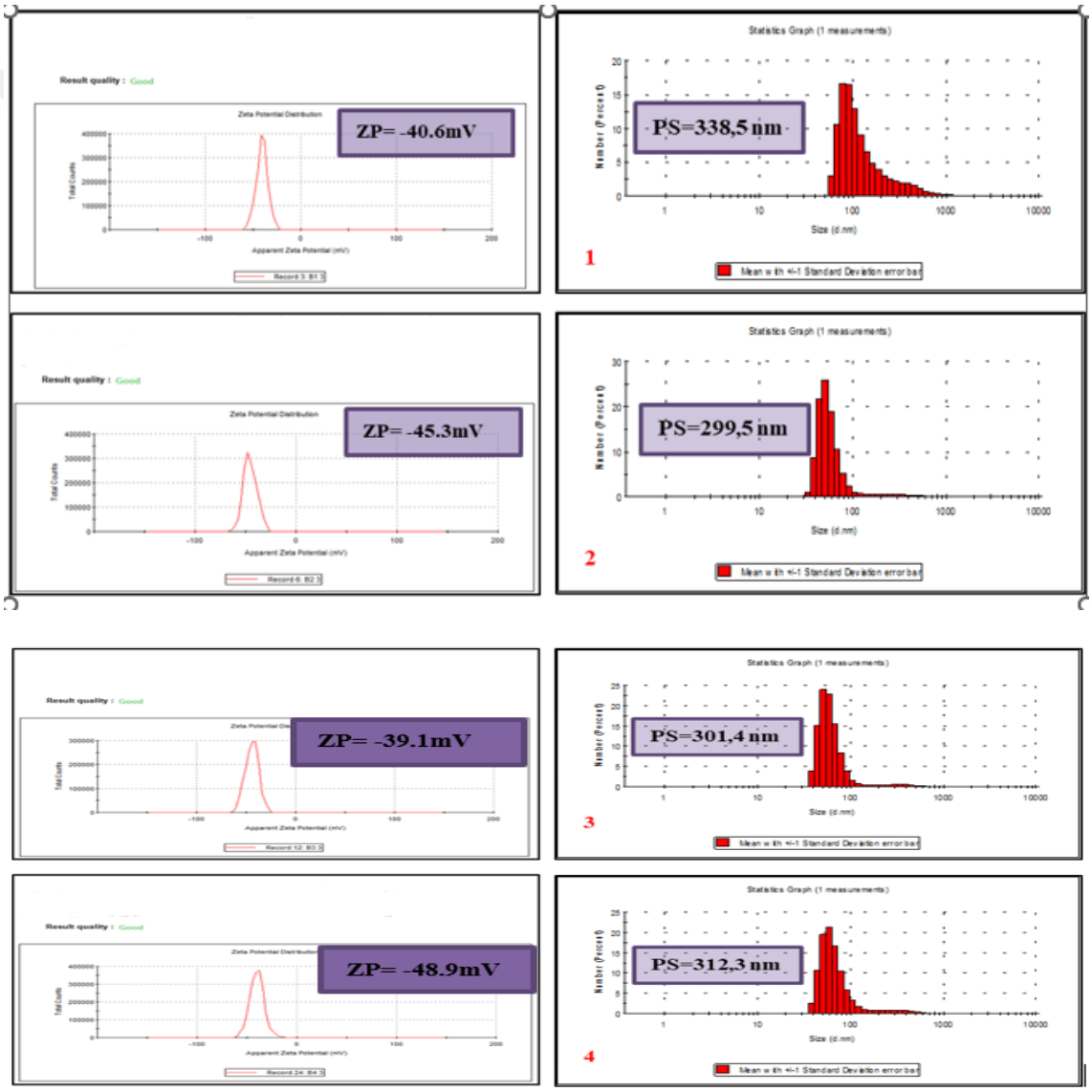

Figure 4.8 ZETA-SIZER spectra (1-4) of graphene oxide samples at the end of the L_9 (3^4) experimental design

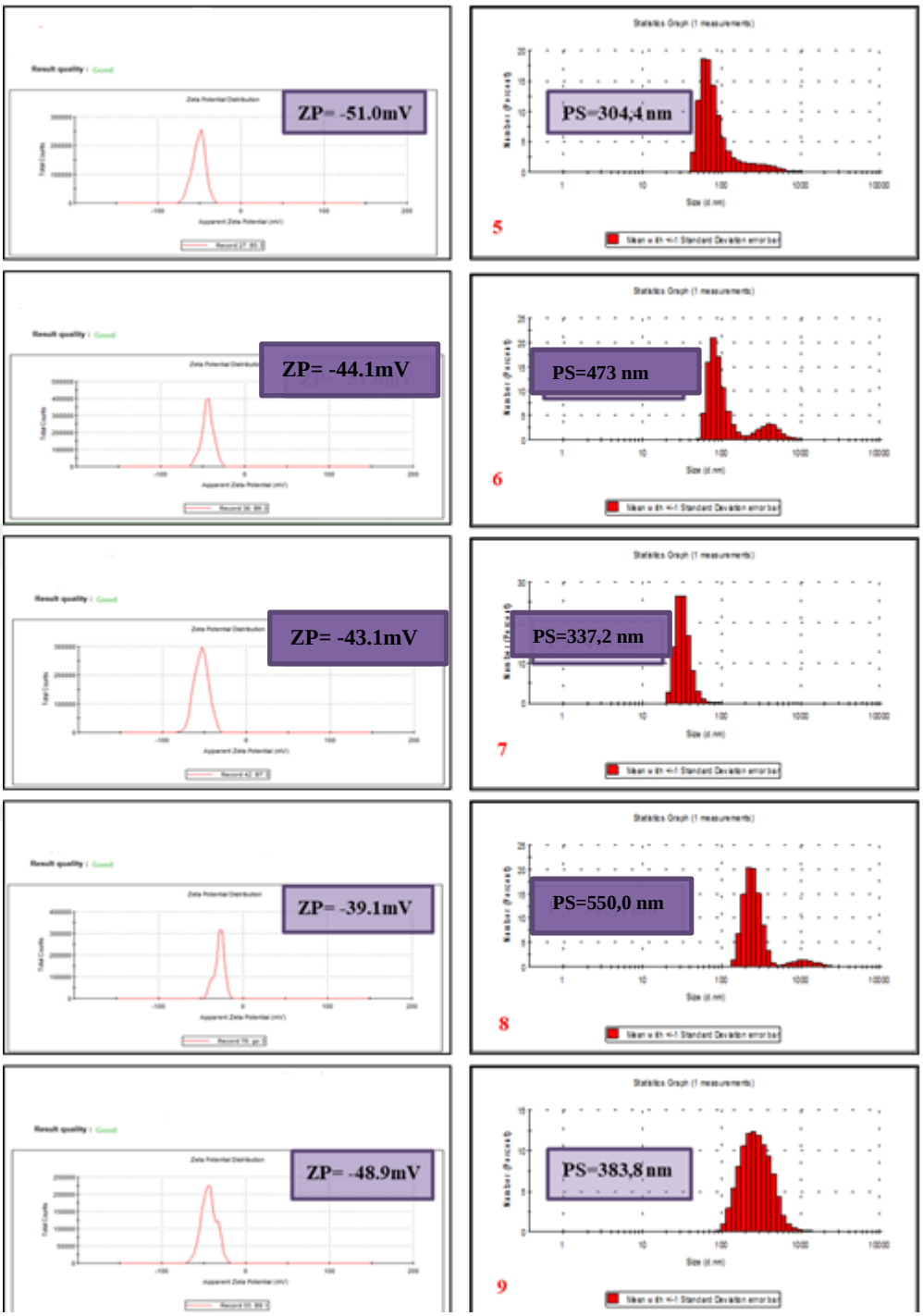

Figure 4.8 ZETA-SIZER spectra (5-9) of graphene oxide samples at the end of the L_9 (3^4) experimental design (Continued**)**

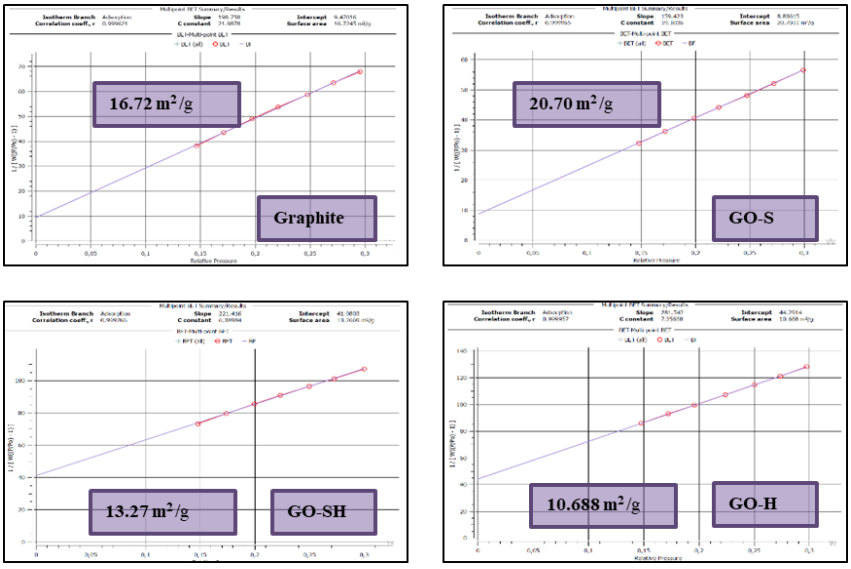

Figure 4.9 BET graphs of graphene oxide samples synthesized from graphite using oxidation methods

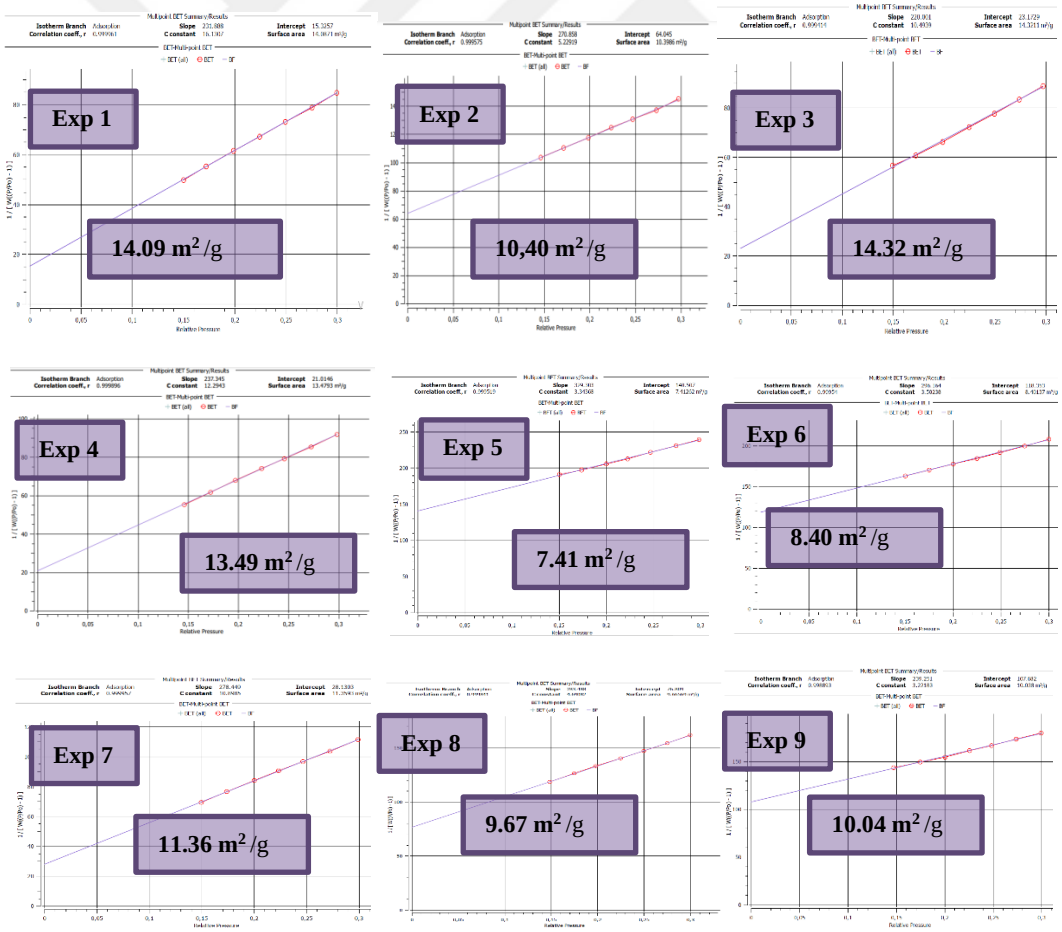

Figure 4.10 BET graphs of graphene oxide samples at the end of the L_9 (3^4) experimental design

In Figures 4.7 and 4.8, the results of Zeta Potential measurements and Particle Size Distribution measurements are presented. The Zeta potential results varied between -37 mV and -53.5 mV. Particle size values ranged from 550 nm to 300 nm. When examining the particle size graphs, it is observed that the graphene oxide samples have reached nano size. In Figure 4.9, BET graphs of Graphene Oxide samples synthesized from graphite using oxidation methods are given. It is observed that the surface area value of the Staudenmaier method is better compared to other methods. The results in the L_9 (3^4) experimental design vary between 7.41 m^2/g and 18.60 m^2/g.

4.2 Optimization of Quality Criterion Using Taguchi Method

In this part of the study, graphene oxide samples were synthesized using the Staudenmaier, Staudenmaier – Modified Hummers, and Modified Hummers methods. The aim is to analyze the effect of boron acid removal using graphene oxide samples synthesized with these three different methods within the experimental design.

Table 4.1 Repetitive results for C/O, D/G, SA, PB, ZP, and H_3BO_3 of graphene oxide samples in the L_9 (3^4) experimental design

Sample	C/O			S.A (m^2/g)		D/G	
	Serial 1	**Serial 2**	**Serial3**	**Serial 1**	**Serial 2**	**Serial 1**	**Serial 2**
Grpht	85.21	50.55	62.29	15.98	14.05	2.88	2.83
GO-S	1.92	1.82	2.26	7.08	8.28	0.92	0.93
GO-SH	1.69	1.36	1.42	11.05	12.03	0.85	0.84
GO-H	1.81	1.45	1.46	21.77	21.37	1.01	1.01
GO-1	1.69	1.73	1.71	11.43	14.09	0.91	0.91
GO-2	1.56	1.67	1.22	10.39	14.99	1.04	1.04
GO-3	1.02	0.94	0.82	16.01	14.32	1.09	1.07
GO-4	1.38	1.35	1.49	9.84	13.49	0.96	0.91
GO-5	1.4	1.3	1.3	6.13	7.41	0.97	0.96
GO-6	1.11	1.34	1.3	13.15	8.4	1.09	1.07
GO-7	1.45	1.41	1.41	9.94	11.36	0.95	0.93
GO-8	1.08	1.18	1.13	7.61	9.67	1.05	1.1
GO-9	1.15	1.21	1.15	7.68	10.03	1.03	1.07

Sample	PB (nm)			ZP (mV)			H_3BO_3(mg)/GO(g)	
	Serial 1	**Serial 2**	**Serial 3**	**Serial 1**	**Serial 2**	**Serial 3**	**Serial 1**	**Serial 2**
Grpht	304.2	399.9	483	-21.3	-23.3	-24.2	N/A	N/A
GO-S	197.6	189.1	206	-34.6	-37.4	-38.2	N/A	N/A
GO-SH	282.5	300	287.3	-38.6	-42.7	-40.4	N/A	N/A
GO-H	312.8	336.3	379.3	-49	-52.3	-51.2	N/A	N/A
GO-1	356.6	345.9	338.5	-38.2	-39.7	-40.6	45.74	45.74
GO-2	294.2	290.4	299.5	-45.3	-45.3	-43.5	69.96	69.96
GO-3	300.5	302.7	301.4	-39	-42.1	-44.1	66.37	66.37
GO-4	312.6	310	312.3	-39.4	-41.3	-40.1	142.61	138.58
GO-5	301.2	308.7	304.4	-48.9	-50.5	-51	32.83	32.83
GO-6	469	474.1	473	-40.8	-43.7	-44.1	118.4	118.4
GO-7	335.4	345.4	337.2	-43.1	-48.9	-53.5	139.92	141.72
GO-8	500	510	550	-39.1	-37.9	-37	209.88	244.86
GO-9	401.7	405.5	383.8	-50.1	-51	-48.9	41.71	39.02

Quality criteria have been established with the aim of identifying the variations in graphene oxide samples after the experiment. Table 4.1 presents the results, along with their repetitions, for the graphene oxide samples obtained at the end of the experiment using the L_9 (3^4) experimental design. This includes the C/O ratio obtained through SEM-EDX analysis, the D/G peak results from RAMAN analysis, surface area (SA) measurements using BET device, particle size distribution (PSD) and zeta potential (ZP) analysis results from ZETA-SIZER analysis. Additionally, the results for the removal of boric acid (H_3BO_3(mg)/GO(g)) obtained at the end of the experiment using the L_9 (3^4) design are also provided with their repetitions.

4.2.1 Optimization Results for Graphene Oxide Samples at the End of the L_9 (3^4) Experimental Design Using the Taguchi Method

As a result of the experiments conducted, the results related to quality criteria in graphene oxide synthesis have been calculated using S/N ratios with the Taguchi Method, as per Equations 1.1-1.2. The data in Tables 4.1 and 4.2 have been analyzed according to the Taguchi Method, and the signal/noise ratio graphs for quality criteria are provided in Figures 4.11-4.16.

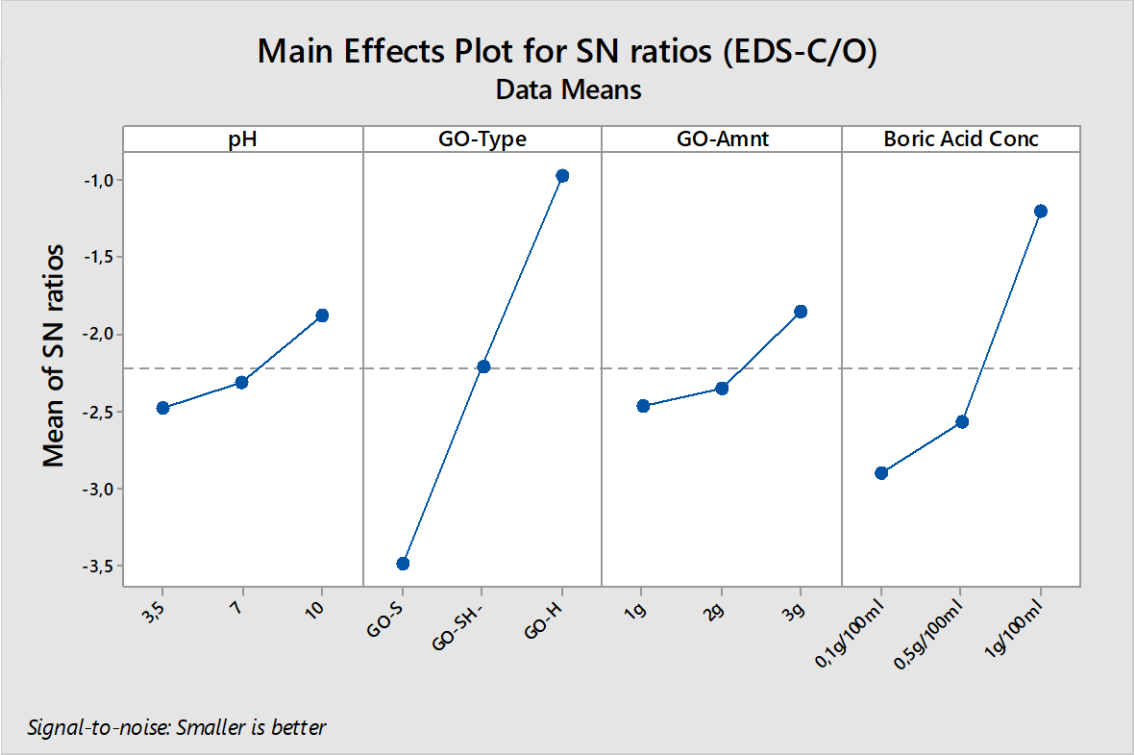

Figure 4.11 The main effect plots of the S/N values for EDS-C/O results obtained using the Taguchi method for the L_9 (3^4) experimental design

When examining the results in Figure 4.11, it can be observed that the C/O ratios from the SEM+EDS analysis of graphene oxide samples vary with the levels of the parameters. The best value for pH has been observed to be 10. This can be attributed to the increase in the number of oxygen-containing groups bound to the structure as the pH increases. The best value for GO-Type has been observed in the Hummers method. In the Hummers method, it indicates that functional groups are more easily attached to the

structure compared to other methods. The best value for GO-Amnt has been observed to be 3g. The increase in the amount of graphene oxide in the environment has led to an increase in the number of oxygen-containing groups attached to the structure. The increase in the concentration of the boric acid solution has also caused an increase in the oxygen-containing groups attached to the structure. The optimum conditions for the EDS-C/O results according to the Taguchi method have been found to be pH: 10, GO-Type: Hummers, GO-Amnt: 3g, and Boric Acid Conc: 1g/100 mL.

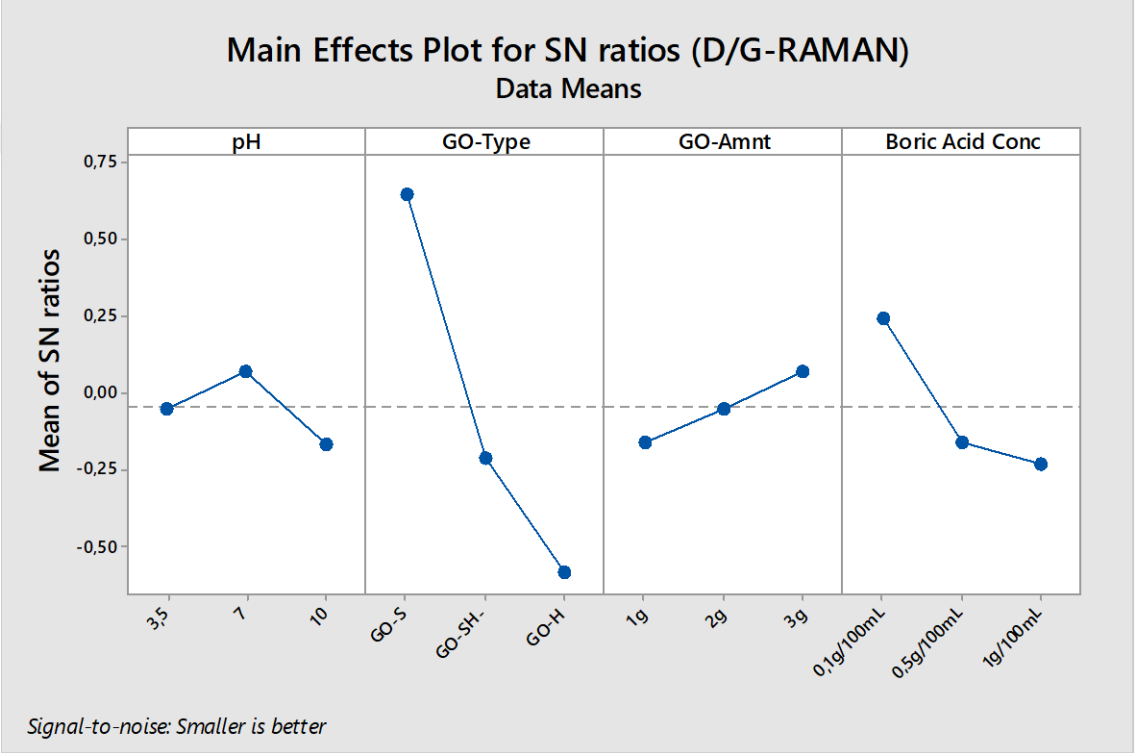

Figure 4.12 The main effect plots of the S/N values for RAMAN-D/G results obtained using the Taguchi method for the L_9 (3^4) experimental design

In Figure 4.12, when the results are examined, it is observed that the D/G ratios for the RAMAN analysis of graphene oxide samples change with the levels in the parameters. No significant change in D/G ratios has been observed as the pH increases. The optimum point for GO-Type has been observed in the Staudenmaier method. The best value for GO-Amnt has been observed to be 3g. As the amount of graphene oxide increases, the defect affecting the structure have decreased. The best value for Boric Acid Conc has been found to be 0.1g/100 mL. An increase in boric acid concentration has caused an increase in defect ratios in the structure, which is attributed to the boric

acid bound to the structure. The optimum conditions for the RAMAN-D/G results according to the Taguchi method have been found to be pH: 7, GO-Type: Staudenmaier, GO-Amnt: 3g, and Boric Acid Conc: 0.1g/100 mL.

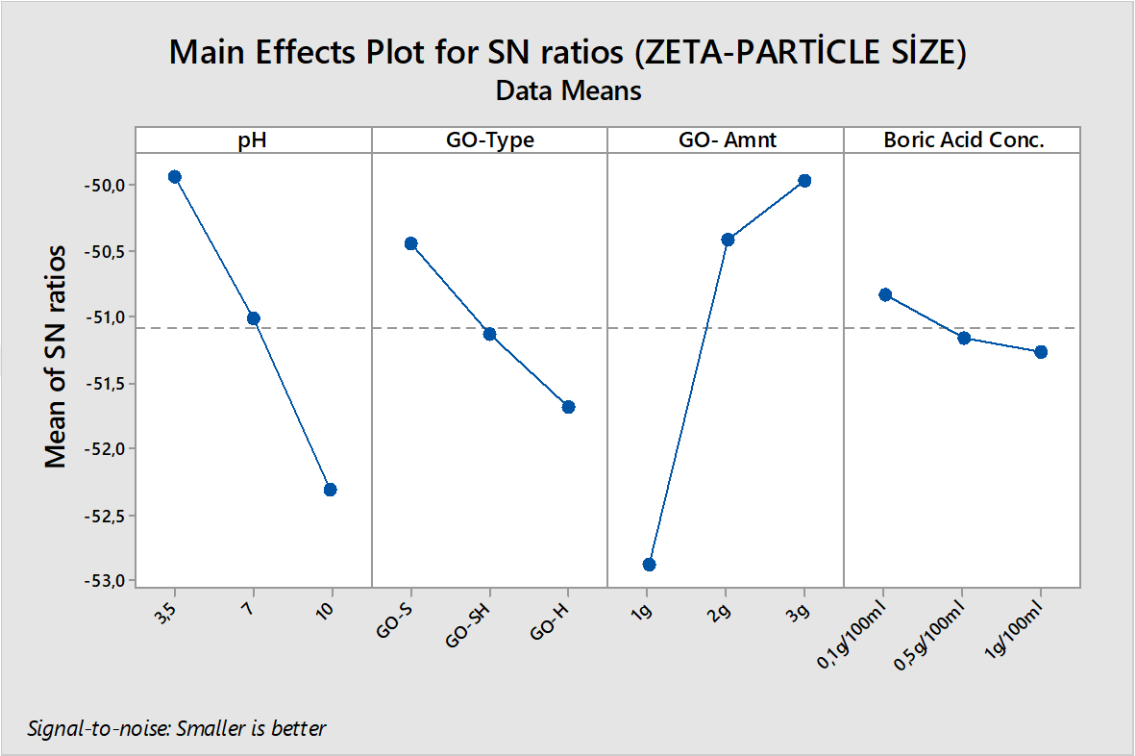

Figure 4.13 The main effect plots of the S/N values for ZETA-PARTICLE SIZE results obtained using the Taguchi method for the L_9 (3^2) experimental design

In Figure 4.13, when the results are examined, it is observed that the Particle-Size results for the ZETASIZER analysis of graphene oxide samples change with the levels of the parameters. The particle size increased as the pH increased. The smallest particle size for GO-Type has been observed in the Staudenmaier method. As the amount of graphene oxide increases, the particle size has decreased. The best value for GO-Amnt has been observed to be 3g. As the concentration of boric acid in the environment increases, the particle size has increased. The best value for Boric Acid Conc has been found to be 0.1g/100 mL. The optimum conditions for the ZETA-PARTICLE SIZE results according to the Taguchi method have been found to be pH: 3.5, GO-Type: Staudenmaier, GO-Amnt: 3g, and Boric Acid Conc: 0.1g/100 mL.

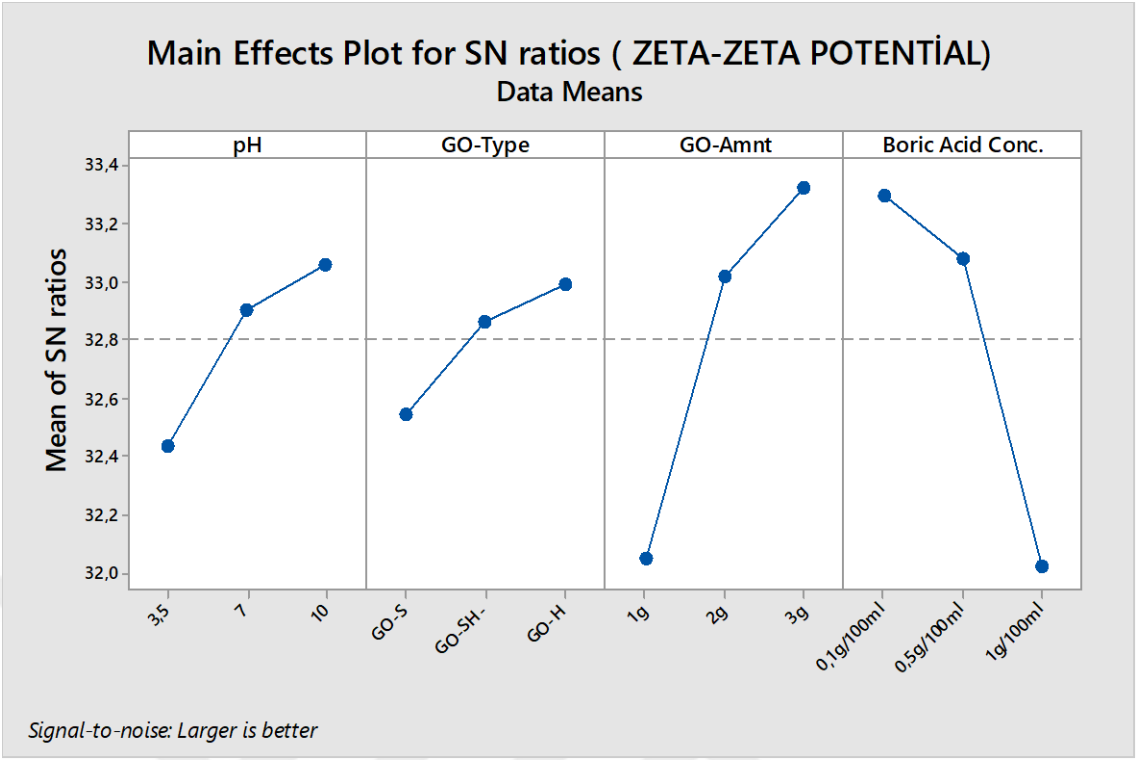

Figure 4.14 The main effect plots of the S/N values for ZETA POTENTIAL results obtained using the Taguchi method for the L_9 (3^4) experimental design

In Figure 4.14, it is observed that the ZETA POTENTIAL results for the ZETA-SIZER analysis of graphene oxide samples change with the levels of the parameters. An increase in pH has been observed to positively affect the ZETA POTENTIAL values. The best values for GO-Type have been observed in the Hummers method. An increase in the amount of Graphene Oxide has improved the Zeta Potential values. The best value for GO-Amnt has been observed to be 3g. An increase in the concentration of boric acid in the environment has negatively affected the Zeta Potential values. The best value for Boric Acid Conc has been found to be 0.1g/100 mL. The optimum conditions for the ZETA-POTENTIAL results according to the Taguchi method have been found to be pH: 3.5, GO-Type: Hummers, GO-Amnt: 3g, and Boric Acid Conc: 0.1g/100 mL.

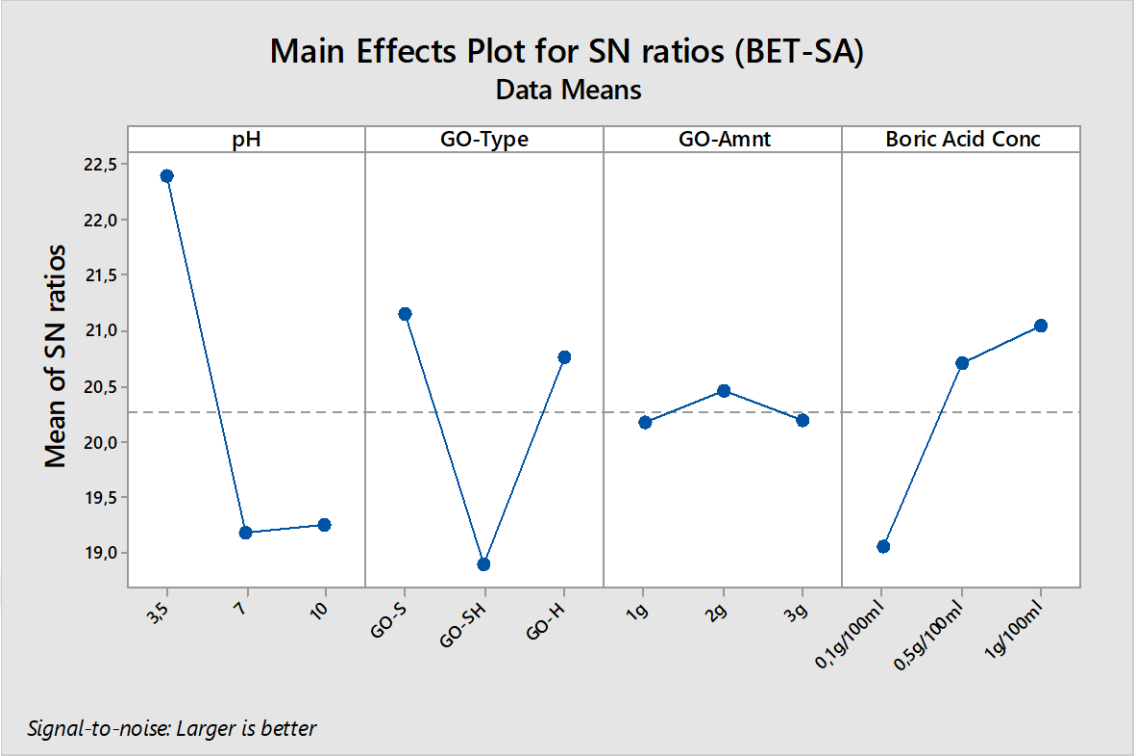

Figure 4.15 The main effect plots of the S/N values for BET-SA (Brunauer-Emmett-Teller Surface Area) results obtained using the Taguchi method for the L_9 (3^2) experimental design

In Figure 4.15, it is observed that the Surface Area results from the BET analysis of graphene oxide samples change with the levels of the parameters. An increase in pH has been observed to negatively affect the Surface Area values. No significant change has been observed for GO-Type and GO-Amnt. An increase in boric acid concentration has shown an enhancing effect on the surface areas of graphene oxide samples. The best value for Boric Acid Conc has been found to be 1 g/100 mL. The optimum conditions for the BET-SA results according to the Taguchi method have been found to be pH: 3.5, GO-Type: Hummers, GO-Amnt: 2g, and Boric Acid Conc: 1g/100 mL.

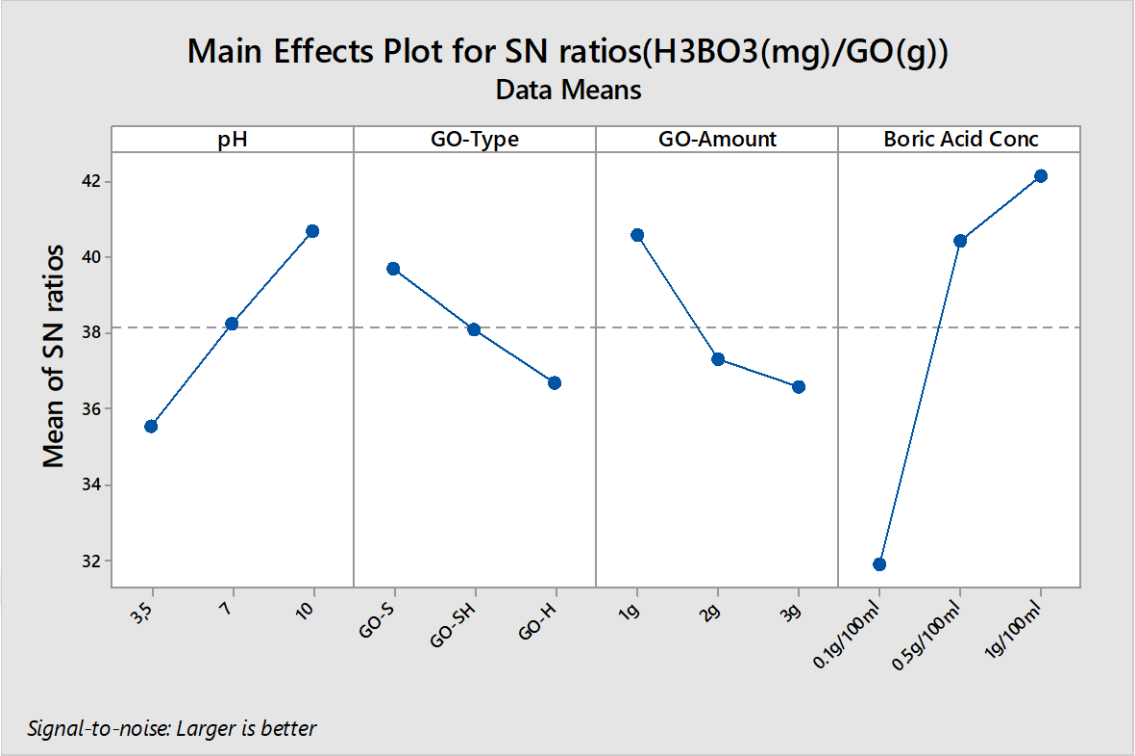

Figure 4.16 The main effect plots of the S/N values for H_3BO_3(mg)/GO(g)-concentration results obtained using the Taguchi method for the L_9 (3^2) experimental design

In Figure 4.16, it is observed that the outcomes of boric acid analyses conducted for the removal of boric acid in boric acid solutions change with the levels of the parameters. Increased boric acid removal has been observed with an increase in pH. The best boric acid removal has been observed in the Staudenmaier method for GO-Type. As the amount of Graphene Oxide increases, the amount of boron per gram has decreased. As the concentration of boric acid in the environment increases, the amount of removed boric acid has increased. The optimum conditions for the H_3BO_3(mg)/GO(g)-Removal results according to the Taguchi method have been found to be pH: 10, GO-Type: Staudenmaier, GO-Amnt: 1g, and Boric Acid Conc: 1g/100 mL.

5. CONCLUSION

In this thesis, an L_9 (3^4) experimental design was conducted for the removal of boric acid, and after the experimental design, six quality criteria were selected for the characterization of graphene oxide samples as given in Table 4.1, and the characterization was performed using the Taguchi method.

- When the results obtained are evaluated in terms of boron removal, it has been observed that boron removal increased with the increase in pH. The adsorption amount increased as the environmental conditions became more basic. This result is also consistent with the literature. In terms of the type of graphene oxide, the best boron adsorption performance was observed in the Staudenmaier method. Although the Hummers method is commonly preferred in the literature, the high boron acid adsorption in the Staudenmaier method has been a notable result. As the amount of graphene oxide increases, the amount of boron acid adsorbed increases, but since the results in our study were characterized based on the amount of boric acid adsorbed per gram of graphene oxide, the amount of boric acid adsorbed per gram decreased as the amount of graphene oxide increased. This was an expected result. As the concentration of boric acid in the solution increased, the amount of boric acid adsorbed per gram of graphene oxide increased. This was also an expected result. The most noteworthy result in the boron removal design was that the performance of the Staudenmaier method was better than the Hummers method. The differences in chemicals between the two methods have caused differences in the structure of graphene oxide, which in turn affected the adsorption performances in boron acid removal. It has been observed that even the use of graphene oxide alone, without forming a composite material, is effective in boron removal.

- When the results obtained are evaluated in terms of the properties of graphene oxide, it has been observed that the surface area values were negatively affected by the increase

in pH, but conversely, the increase in boric acid concentration had a positive effect on the surface area values. For zeta potential values, the increase in pH and the amount of graphene oxide had a positive effect, while the increase in boric acid concentration had a negative effect. For zeta potential values, the Hummers method was more effective compared to the other two methods. For particle size values, the increase in pH and boric acid concentration negatively affected the particle size values. It can be said that the boric acid used here is not of a nano-featured structure. The increase in the amount of graphene oxide had a positive effect on particle size values. The reason for this can be attributed to the nano-featured structure of the graphene oxide samples used, as shown in Figure 4.13. The fact that the Staudenmaier method contains more nano-featured particles compared to other methods is consistent with the optimization results. When the Raman analysis results are evaluated, no effective change was observed in the D/G values with the increase in pH. The increase in the amount of graphene oxide had a positive effect on the D/G values. The best result among the methods was given by the Staudenmaier method. The increase in boric acid concentration negatively affected the D/G values. This may be due to the formation of an irregular structure caused by the boric acid bonds attached to the structure. When the optimization results for the C/O ratio criterion are evaluated, the increase in pH and thus the increase in OH ions, the increase in the amount of graphene oxide and thus the increase in the amount of added NaOH, and the increase in boric acid concentration and thus the increase in oxygen-containing structures added to the structure, had a positive effect on the C/O ratios.

As a conclusion, if all the results obtained from the study are considered, graphene oxide has been seen to be a good adsorbent for boron removal. Additionally, boric acid has shown improving effects on the structure of graphene oxide and has been incorporated into its structure. The use of graphene oxide for the valorization of boron wastes and the enhancing effects on the properties of graphene oxide has been an interesting study.

REFERENCES

Abd Mutalib, M., Rahman, M. A., Othman, M. H. D., Ismail, A. F. and Jaafar, J. 2017. Scanning electron microscopy (SEM) and energy-dispersive X-ray (EDX) spectroscopy. Membrane Characterization, 7: 161-179.

Abedi, M., Fangueiro, R. and Correia, A. G. 2021. A review of intrinsic self-sensing cementitious composites and prospects for their application in transport infrastructures. Construction and Building Materials, 310: 125139.

Ahmad, S., Mustonen, K., McLean, B., Jiang, H., Zhang, Q., Hussain, A., Khan, A. T., Ding, E. X., Liao, Y., Wei, N., Monazam, M. R. A., Nasibulin, A. G., Kotakoski, J., Page, A. J. and Kauppinen, E. I. 2020. Hybrid low-dimensional carbon allotropes formed in gas phase. Advanced Functional Materials, 30(45): 2005016.

Ahmed, A., Singh, A., Young, S. J., Gupta, V., Singh, M. and Arya, S. 2023. Synthesis techniques and advances in sensing applications of reduced graphene oxide (rGO) Composites: A review. Composites Part A: Applied Science and Manufacturing, 165: 107373.

Al-Afy, N. and Sereshti, H. 2019. Rapid removal of boron from environmental water samples using magnetic graphene oxide: Optimized by central composite design. Desalination and Water Treatment, 153: 65–75.

Bademlioglu, A. H., Canbolat, A. S. and Kaynakli, O. 2020. Multi-Objective Optimization of Parameters Affecting Organic Rankine Cycle Performance Characteristics with Taguchi-Grey Relational Analysis. Renewable and Sustainable Energy Reviews, 117: 109483.

Bentedlaouti, K., Belouatek, A. and Kebaili, N. 2024. Antibacterial and antioxidant activities of graphene and graphene oxide synthesis coated silver nanoparticules. Journal of Crystal Growth, 627: 127527.

Berthomieu, C. and Hienerwadel, R. 2009. Fourier transform infrared (FTIR) spectroscopy. Photosynthesis research, 101: 157-170.

Brdar-Jokanović, M. 2020. Boron toxicity and deficiency in agricultural plants. International journal of molecular sciences, 21(4): 1424

Canıyılmaz, E. 2001. Kalite Geliştirmede Taguchi Metodu ve Bir Uygulama. MSc. Thesis, Gazi Üniversitesi, Ankara.

Çelikoyan, B. K. 2008. Kolemanitten Propiyonik Asit Varlığında Borik Asit Üretim Prosesinden Geliştirilmesi. Doctoral dissertation, 170 page, İstanbul Teknik Üniversitesi.

Chaloupková, Z., Žárská, L., Belza, J. and Poláková, K. 2023. Label-free detection and mapping of graphene oxide in single HeLa cells based on MCR-Raman spectroscopy. Analytical Methods, 15(42): 5582-5588.

Chapin, R. E. and Ku, W. W. 1994. The Reproductive Toxicity of Boric Acid. Environmental Health Perspectives 102(7): 87–91.

Chen, F., Guo, L., Zhang, X., Leong, Z. Y., Yang, S. and Yang, H. Y. 2017. Nitrogen-doped graphene oxide for effectively removing boron ions from seawater. Nanoscale, 9(1): 326–333.

Chen, M., Dollar, O., Shafer-Peltier, K., Randtke, S., Waseem, S. and Peltier, E. 2020. Boron removal by electrocoagulation: Removal mechanism, adsorption models and factors influencing removal. Water Research, 170: 115362.

Chen, T., Wang, Q., Lyu, J., Bai, P. and Guo, X. 2020. Boron removal and reclamation by magnetic magnetite (Fe_3O_4) nanoparticle: An adsorption and isotopic separation study. Separation and Purification Technology, 231: 115930.

Chen, Y., Lyu, J., Wang, Y., Chen, T., Tian, Y., Bai, P. and Guo, X. (2019). Synthesis, Characterization, Adsorption, and Isotopic Separation Studies of Pyrocatechol-Modified MCM-41 for Efficient Boron Removal. Industrial and Engineering Chemistry Research, 58(8): 3282–3292.

Dai, D., Li, Y. and Fan J. 2021. Room-temperature synthesis of various allotropes of carbon nanostructures (graphene, graphene polyhedra, carbon nanotubes and nano-onions, n-diamond nanocrystals) with aid of ultrasonic shock using ethanol and potassium hydroxide. Carbon, 179: 133-141.

Demirel, H., Taylan, İ. N. C. E., Uysal, D. and UYSAL, B. (2015). Boric Acid Production From Sodium Metaborate With Sulfuric Acid. Celal Bayar University Journal of Science, 11(3): 379–82.

Elevli, B., Yaman, İ. and Laratte, B. 2022. Estimation of the Turkish boron exportation to Europe. Mining, 2(2): 155-169.

Erkan, N. 2002. Boraks Dekahidrat Kristalizasyonu Üzerine Safsızlıkların Etkisi. Doctoral dissertation, İstanbul Teknik Üniversitesi 75 sayfa, İstanbul.

Fardinpour, P., Ghafouri Taleghani, H. and Reza Zakerimehr, M. 2024. Facile green synthesis of graphene oxide/copper oxide nanocomposites using ginger essential oil and its enhanced antibacterial properties. Materials Science and Engineering: B, 300: 117100.

Farjadian, F., Abbaspour, S., Sadatlu, M. A. A., Mirkiani, S., Ghasemi, A., Hoseini-Ghahfarokhi, M., Mozaffari, N., Karimi, M. and Hamblin, M. R. 2020. Recent developments in graphene and graphene oxide: Properties, synthesis, and modifications: A review. ChemistrySelect, 5(33): 10200-10219.

Geim, Andre K. and Philip Kim. 2008. Carbon. Scientific American (April):90–97.

Georgakilas, V., Tiwari, J. N., Kemp, K. C., Perman, J. A., Bourlinos, A. B., Kim, K. S. and Zboril, R. 2016. Noncovalent functionalization of graphene and graphene oxide for energy materials, biosensing, catalytic, and biomedical applications. Chemical reviews, 116(9): 5464-5519.

Guo, Q., Zhang, Y., Cao, Y., Wang, Y. and Yan, W. 2013. Boron sorption from aqueous solution by hydrotalcite and its preliminary application in geothermal water deboronation. Environmental Science and Pollution Research, 20(11): 8210–8219.

Habte, A. T. and Ayele, D. W. 2019. Synthesis and characterization of reduced graphene oxide (rGO) started from graphene oxide (GO) using the tour method with different parameters. Advances in Materials Science and Engineering https://doi.org/10.1155/2019/5058163

Hadrup, N., Frederiksen, M. and Sharma, A. K. 2021. Toxicity of boric acid, borax and other boron containing compounds: A review. Regulatory toxicology and pharmacology, 121: 104873.

Honda, S. I., Higo, Y., Niwase, K., Niibe, M., Terasawa, M., Taguchi, E. and Nakamura, S. 2021. In situ observation of transformation of neutron-irradiated highly oriented pyrolytic graphite (HOPG) by X-ray diffraction under high-pressure and high-temperature treatment. Japanese Journal of Applied Physics, 60(9): 095002.

Hu, G., Zhang, W., Chen, Y., Xu, C., Liu, R. and Han, Z. 2020. Removal of boron from water by GO/ZIF-67 hybrid material adsorption. Environmental Science and Pollution Research, 27(22): 28396–28407.

Hummers Jr, W. S. and Offeman, R. E. 1958. Preparation of graphitic oxide. Journal of the american chemical society, 80(6): 1339-1339.

İnal, V. 2009. Kolemanitin Nitrik Asit Çözeltilerinde Çözünme Kinetiği. Yüzüncü Yıl Üniversitesi, 55 sayfa, Van.

İpekçi, D., Kabay, N., Bunani, S., Altıok, E., Arda, M., Yoshizuka, K. and Nishihama, S. 2020. Application of heterogeneous ion exchange membranes for simultaneous separation and recovery of lithium and boron from aqueous solution with bipolar membrane electrodialysis (EDBM). Desalination, 479:114313

Jia, Y., Zhang, J., Kong, D., Zhang, C., Han, D., Han, J., Tao, Y. and Yang, Q. H. 2022. Practical graphene technologies for electrochemical energy storage. Advanced Functional Materials, 32(42): 2204272.

Kamcev, J., Taylor, M. K., Shin, D. M., Jarenwattananon, N. N., Colwell, K. A. and Long, J. R. 2019. Functionalized Porous Aromatic Frameworks as High-Performance Adsorbents for the Rapid Removal of Boric Acid from Water. Advanced Materials, 31(18): 1–9.

Kar, Y., Şen, N. and Demirbaş, A. 2006. Boron minerals in Türkiye, their application areas and importance for the country's economy. Minerals and Energy-Raw Materials Report, 20(3-4), 2-10.

Keshavarz, L., Ghaani, M. R., Saremi, O. and English, N. J. 2022. Characterization of Nanoporous Materials. Advanced Functional Porous Materials: From Macro to Nano Scale Lengths, 319-351.

Kharisov, B. I., Kharissova, O. V., Kharisov, B. I. and Kharissova, O. V. 2019. General data on carbon allotropes. Carbon Allotropes: Metal-Complex Chemistry, Properties and Applications, 1-8

Korkmaz, S. and Kariper, A. 2020. Graphene and graphene oxide based aerogels: Synthesis, characteristics and supercapacitor applications. Journal of Energy Storage, 27:101038

Kumar, N., Verma, S., Kumar, P., Ahmad, A., Park, J. and Chandra, V. 2024. Efficient one-pot two-step electrochemical synthesis of highly oxidized graphene oxide for enhanced energy and environmental applications: Structure elucidation through DFT simulations. Carbon, 218 : 118722.

Kunkel, M., Bitter, S., Sailer, F., Winter, R. F. and Polarz, S. 2020. Aggregation-Induced Improvement of Catalytic Activity by Inner-Aggregate Electronic Communication of Metal-Fullerene-Based Surfactants. ChemCatChem, 12(10): 2726-2731.

Lan, N., Wang, K. Y., Weber, M., Maletzko, C. and Chung, T. S. 2021. Investigation of novel molecularly tunable thin-film nanocomposite nanofiltration hollow fiber membranes for boron removal. Journal of Membrane Science, 620:118887.

Lin, M.C., Qiu, G.P., Zhou, X.H. and Chen, C.N., 2020. Using Taguchi and neural network approaches in the optimum design of product development process. International Journal of Computer Integrated Manufacturing, 33(4), pp.343-359.

Lin, T., Zhang, Y. Q., Zhang, L. and Klappenberger, F. 2018. On-Surface Chemistry of Alkyne Derivatives. Encyclopedia of Interfacial Chemistry, 324-334.

Lyu, J., Liu, H., Zhang, J., Zeng, Z., Bai, P. and Guo, X. 2017. Metal-organic frameworks (MOFs) as highly efficient agents for boron removal and boron isotope separation. RSC Advances, 7(26): 16022–16026.

Mermer, C. and Şengül, H. 2020. Addressing potential resource scarcity for boron mineral: A system dynamics perspective. Journal of Cleaner Production, 270: 122192.

Merodio-Perea, R. G., Lado-Touriño, I., Páez-Pavón, A., Talayero, C., Galán-Salazar, A. and Aït-Salem, O. 2022. Mechanical properties of cement reinforced with pristine and functionalized carbon nanotubes: Simulation studies. Materials, 15(21): 7734.

Mumcu, H. 2010. Kolemanitin Sodyumbisülfat Çözeltilerinde Çözünme Kinetiğinin Incelenmesi, Doctoral dissertation, 76 page, Y Atatürk Üniversitesi.

Muniyalakshmi, M., Sethuraman, K., and Silambarasan, D. 2020. Synthesis and characterization of graphene oxide nanosheets. Materials Today: Proceedings, 21: 408–410.

Muzyka, R., Kwoka, M., Smędowski, Ł., Díez, N. and Gryglewicz, G. 2017. Oxidation of graphite by different modified Hummers methods. New Carbon Materials, 32(1): 15-20.

Özkurt, Ö. 1999. Deney Tasarımları ve Istatistiksel Veri Analizi, Doctoral dissertation, İstanbul Teknik Üniversitesi, İstanbul.

Pan, Y., Liu, X., Zhang, W., Liu, Z., Zeng, G., Shao, B., Liang, Q., He, Q., Yuan, X., Huang, D. and Chen, M. 2020. Advances in photocatalysis based on fullerene C60 and its derivatives: Properties, mechanism, synthesis, and applications. Applied Catalysis B: Environmental, 265: 118579.

Patel, N.S., Parihar, P.L. and Makwana, J.S., 2021. Parametric optimization to improve the machining process by using Taguchi method: a review. Materials Today: Proceedings, 47, pp.2709-2714.

Prasad Nayak, S., Swarnkar, N. and Kiran Kumar, J. K. 2024. Eco-friendly synthesis of reduced graphene oxide as sustainable catalyst for photodegradation of methylene blue. Inorganic Chemistry Communications, 159(November 2023): 111792.

Rahman, M. M., Shafiullah, A. Z., Pal, A., Islam, M. A., Jahan, I. and Saha, B. B. 2021. Study on optimum IUPAC adsorption isotherm models employing sensitivity of parameters for rigorous adsorption system performance evaluation. Energies, 14(22): 7478.

Shnoudeh, A. J., Hamad, I., Abdo, R. W., Qadumii, L., Jaber, A. Y., Surchi, H. S. and Alkelany, S. Z. 2019. Synthesis, characterization, and applications of metal nanoparticles. Biomaterials and bionanotechnology, 527-612.

Shojaeenezhad, S. S., Farbod, M. and Kazeminezhad, I. 2017. Effects of initial graphite particle size and shape on oxidation time in graphene oxide prepared by Hummers' method. Journal of Science: Advanced Materials and Devices, 2(4): 470-475.

Şimsek, B. 2014. Hazır Betonun Optimal Karışım Oranlarının Belirlenmesi Için Birçok Yanıtlı Modelleme ve Eniyileme Uygulaması: Topsıs Tabanlı Taguchi Yaklaşımı Ile Cevap Yüzey Yöntemi. Ankara Üniversitesi, 221 sayfa, Ankara.

Sokmen, N. and Buyukakinci, B. Y. 2018. The usage of boron/boron compounds in the textile industry and its situation in Türkiye. CBU International Conference Proceedings, 6: 1158-1165.

Song, S., Shen, H., Wang, Y., Chu, X., Xie, J., Zhou, N. and Shen, J. 2020. Biomedical application of graphene: From drug delivery, tumor therapy, to theranostics. Colloids and Surfaces B: Biointerfaces, 185: 110596.

Tang, Y. P., Chung, T. S., Weber, M. and Maletzko, C. 2017. Development of Novel Diol-Functionalized Silica Particles toward Fast and Efficient Boron Removal. Industrial and Engineering Chemistry Research, 56(40): 11618–11627.

Taşçı, T., Küçükyıldız, G., Hepyalçın, S., Ciğeroğlu, Z., Şahin, S. and Vasseghian, Y. 2022. Boron removal from aqueous solutions by chitosan/functionalized-SWCNT-COOH: Development of optimization study using response surface methodology and simulated annealing. Chemosphere, 288:132554

Thakur, K. and Kandasubramanian, B. 2019. Graphene and graphene oxide-based composites for removal of organic pollutants: a review. Journal of Chemical and Engineering Data, 64(3): 833-867.

Tolun, R. 1981. Anorganik Bor Bileşikleri ve Üretim Teknolojisi. Tübitak Kimya Araştırma Bölümü, 65 sayfa, Kocaeli.

Turkbay, T., Bongono, J., Alix, T., Laratte, B. and Elevli, B. 2022. Prior knowledge of the data on the production capacity of boron facilities in Türkiye. Cleaner Engineering and Technology, 10: 100539.

Wang, H.K., Wang, Z.H. and Wang, M.C., 2020. Using the Taguchi method for optimization of the powder metallurgy forming process for Industry 3.5. Computers & Industrial Engineering, 148:106635

Wang, Q., Chen, T., Bai, P., Lyu, J. and Guo, X. 2021. Fe3O4-loaded ion exchange resin for chromatographic separation of boron isotopes: Experiment and numerical simulation. Chemical Engineering Research and Design, 171: 358–366.

Yu, P., Tian, Z., Lowe, S. E., Song, J., Ma, Z., Wang, X., Han, Z. J., Bao, Q., Simon, G. P., Li, D. and Zhong, Y. L. 2016. Mechanically-assisted electrochemical production of graphene oxide. Chemistry of Materials, 28(22): 8429-8438.

Yu, W., Sisi, L., Haiyan, Y. and Jie, L. 2020. Progress in the functional modification of graphene/graphene oxide: A review. RSC advances, 10(26): 15328-15345.

CURRICULUM VITAE

Personal Information

Name and Surname : Tabarek Salam Majeed MAJEED

Education

MSc	Çankırı Karatekin University Graduate School of Natural and Applied Sciences Department of Chemical Engineering	2021-2024
Undergraduate	Baghdad University Al-Khwarizmi College of Engineering Department of Biochemical Engineering	2015-2019